





Review

Review on Activated Carbons by Chemical Activation with FeCl₃

Jorge Bedia *, Manuel Peñas-Garzón , Almudena Gómez-Avilés , Juan J. Rodríguez and Carolina Belver *

Departamento de Ingeniería Química, Facultad de Ciencias, Universidad Autónoma de Madrid, Campus Cantoblanco, E-28049 Madrid, Spain; manuel.pennas@uam.es (M.P.-G.); almudena.gomez@uam.es (A.G.-A.); juanjo.rodriguez@uam.es (J.J.R.)

* Correspondence: jorge.bedia@uam.es (J.B.); carolina.belver@uam.es (C.B.);
Tel.: +34-91-497-29-11 (J.B.); +34-91-497-84-73 (C.B.)

Received: 23 March 2020; Accepted: 9 April 2020; Published: 10 April 2020



Abstract: This study reviews the most relevant results on the synthesis, characterization, and applications of activated carbons obtained by novel chemical activation with FeCl₃. The text includes a description of the activation mechanism, which comprises three different stages: (1) intense de-polymerization of the carbon precursor (up to 300 °C), (2) devolatilization and formation of the inner porosity (between 300 and 700 °C), and (3) dehydrogenation of the fixed carbon structure (>700 °C). Among the different synthesis conditions, the activation temperature, and, to a lesser extent, the impregnation ratio (i.e., mass ratio of FeCl₃ to carbon precursor), are the most relevant parameters controlling the final properties of the resulting activated carbons. The characteristics of the carbons in terms of porosity, surface chemistry, and magnetic properties are analyzed in detail. These carbons showed a well-developed porous texture mainly in the micropore size range, an acidic surface with an abundance of oxygen surface groups, and a superparamagnetic character due to the presence of well-distributed iron species. These properties convert these carbons into promising candidates for different applications. They are widely analyzed as adsorbents in aqueous phase applications due to their porosity, surface acidity, and ease of separation. The presence of stable and well-distributed iron species on the carbons' surface makes them promising catalysts for different applications. Finally, the presence of iron compounds has been shown to improve the graphitization degree and conductivity of the carbons; these are consequently being analyzed in energy storage applications.

Keywords: activated carbons; chemical activation; iron chloride; adsorption

1. Activated Carbons

Activated carbons are amorphous carbon materials, mainly characterized by a well-developed porous texture [1]. They are widely used in many different applications including (1) adsorption, both in gas and liquid phases [2–4], (2) catalysis, mostly as supports of the active phases [5–9] but also as bulk catalysts [10–13], and (3) in electrochemical or energy storage applications for use as supercapacitors [14–18]. There is currently a reborn interest in research of the synthesis, characterization, and applications of activated carbons, as shown by recent reviews and the high number of publications on this topic that can be found in the technical literature [19–24]. Activated carbons can be synthesized from any carbonaceous precursor, such as coal [25–27], discarded tires [28–30], lignin [31–33], or biomass waste [34–37], among others, preferably with low inorganic content. Nowadays, most of the research is focused in the synthesis of activated carbons from biomass waste due to some unquestionable advantages: (1) this process results in the revalorization of waste, (2) the synthesized activated carbons have a lower cost since they are produced from low economic value precursors, (3) they are obtained

from renewable resources, and (4) after their lifetime, the combustion of these activated carbons does not increase CO₂ accumulation in the atmosphere because this CO₂ has been previously captured during plant growth [38,39].

There are two different procedures for synthesizing activated carbons, namely physical activation and chemical activation (Figure 1) [1,22]. The former consists of two different thermal steps. The first one is a pyrolysis or carbonization of the carbonaceous precursor at high temperatures, usually in the range of 700–900 °C, under inert atmosphere to avoid combustion on the carbonaceous matter. In this step, heteroatoms are removed and volatiles are released, resulting in chars with high carbon content (the increase of the carbonization temperature increases carbon content) but with still low porosity development. The second step of the physical activation process is gasification. This consists of a selective removal of the most reactive carbon atoms by controlled gasification reactions that generate the characteristic porosity of the activated carbons. The gasification temperature depends on the gasification agent used, usually water vapor, CO₂, or O₂ (air). Temperatures in the range of around 700–900 °C are used with water vapor or CO₂ gasification. In contrast, when using pure O₂ or air, the gasification temperatures should be much lower (around 300–450 °C) due to the much higher reactivity of O₂ than CO₂ and water vapor. Moreover, the use of O₂ hinders the control of the gasification and thus porosity development, due to the high reactivity and exothermicity of the reaction with O₂.

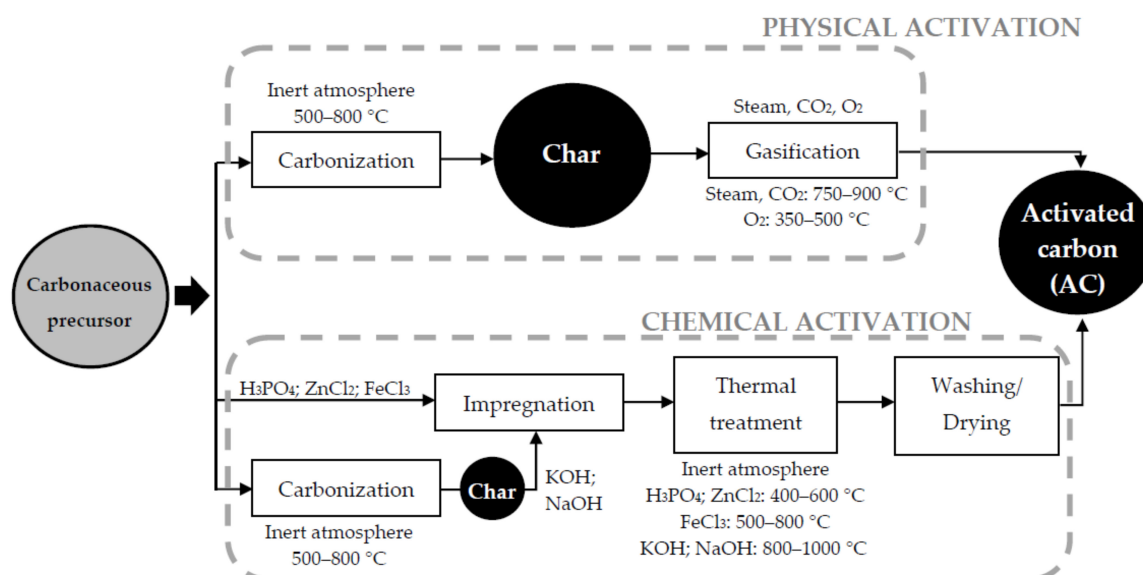


Figure 1. Synthesis of activated carbons (adapted from [22]).

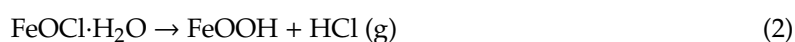
The second procedure for synthesizing activated carbons is chemical activation. This process has only one thermal step, although it indeed consists of three different synthesis stages (Figure 1). The first is the impregnation of the precursor with the activating agent. Different activating agents have been traditionally studied in the literature, such as ZnCl₂, H₃PO₄, NaOH, or KOH, among others. FeCl₃ activation, the subject of this review, has received increasing attention in recent years. The impregnation procedure can be accomplished by different techniques. For example, some authors use an aqueous solution of the activating agent put in contact with the carbonaceous precursor. However, other studies perform a direct and simpler physical mixing of the precursor and the activating agent. Probably one of the most influential synthesis parameters with respect to the texture characteristics of the final activated carbon is the impregnation ratio or mass ratio between the activating agent and the carbonaceous precursor. Impregnation ratios between 0.5 and 5 are most commonly found in the literature. After impregnation, the second step of the chemical activation procedure is thermal treatment in an inert atmosphere at different temperatures depending on the chosen activating agent. The usual temperatures employed depend on the activating agent and are summarized in Figure 1.

During this step, reactions of de-polymerization, dehydration, and condensation take place, resulting in higher carbon yields than in physical activation due to the restriction in the formation of tars and volatiles. Finally, the last stage involves washing to remove the remaining activating agents and reaction byproducts that occlude the newly formed porosity, and drying. In the case of NaOH or KOH activation of “soft” carbon precursors (i.e., biomass waste), an initial carbonization step is usually needed, because otherwise, these strong bases can dissolve the organic matter of the precursor, making the subsequent activation impossible.

In this review, the activation mechanism, synthesis conditions, characterization, and applications of activated carbons obtained by chemical activation with FeCl₃ will be summarized and analyzed. The use of FeCl₃ has some advantages with respect to other more traditional chemical activation agents. For example, it has a lower cost and is more environmentally friendly. Other traditional activating agents, such as KOH, NaOH, or H₃PO₄, are very strong bases and acids. The handling of these materials requires stricter security measures and materials more resistant to corrosion, increasing the cost of the synthesis process. In the case of ZnCl₂, Zn ions and derived oxides are toxic [40,41], and therefore should be submitted to stricter discharge regulations. All these facts mean that FeCl₃ activation can be considered as low cost and environmentally benign in comparison to those traditional activating agents. Another interesting characteristic of this activation procedure is that it can produce magnetic activated carbons [42,43].

2. Activation Mechanism

Xu et al. [44,45] recently analyzed the mechanism of pore formation in the activation of waste cotton with iron chloride. They concluded that the activation process consists of several subsequent stages, as schematized in Figure 2. The presence of iron chloride reduces the temperature of the cellulose hydrolysis and causes an intense de-polymerization reaction with the release of a high amount of low molecular weight hydrocarbons. At pyrolysis temperatures between 200 and 300 °C, iron chlorides break the glycoside bonds of cellulose, and H₂O molecules are simultaneously released from the hydrated salt, resulting in the formation of glucose monosaccharides. In this temperature range, hydrated iron chloride salt decomposes into amorphous FeOOH through the following reactions [46]:



The second stage occurs at pyrolysis temperatures between 330 and 700 °C. As the activation temperature increases, glucose molecules suffer successive ring opening, dehydration, and cyclization into 5-hydroxymethylfurfural, which after decarbonylation is transformed into furfural [47]. With the increase of the temperature, FeOOH is firstly decomposed into Fe₂O₃, which is subsequently reduced by the carbon surface to form Fe₃O₄ according to the following chemical reactions [48]:



These iron oxides catalyze the generation of the microporosity on the carbon matrix [49]. Besides, different hydrocarbons produced during pyrolysis are deposited on the Fe₂O₃ and Fe₃O₄ surfaces and form mesopores after the removal of the iron species in the acid washing step. A further increase of the activation temperature (>700 °C) resulted in an increase of the fixed carbon proportion of the solid while releasing volatile matter, water vapor, and carbon dioxide, as a consequence of the polymerization and polycondensation that occurred between furfural and 5-hydroxymethylfurfural [50,51]. At these high temperatures iron species are reduced to zerovalent iron by the surface of the carbon surface (Equations (5)–(7)) [52]:



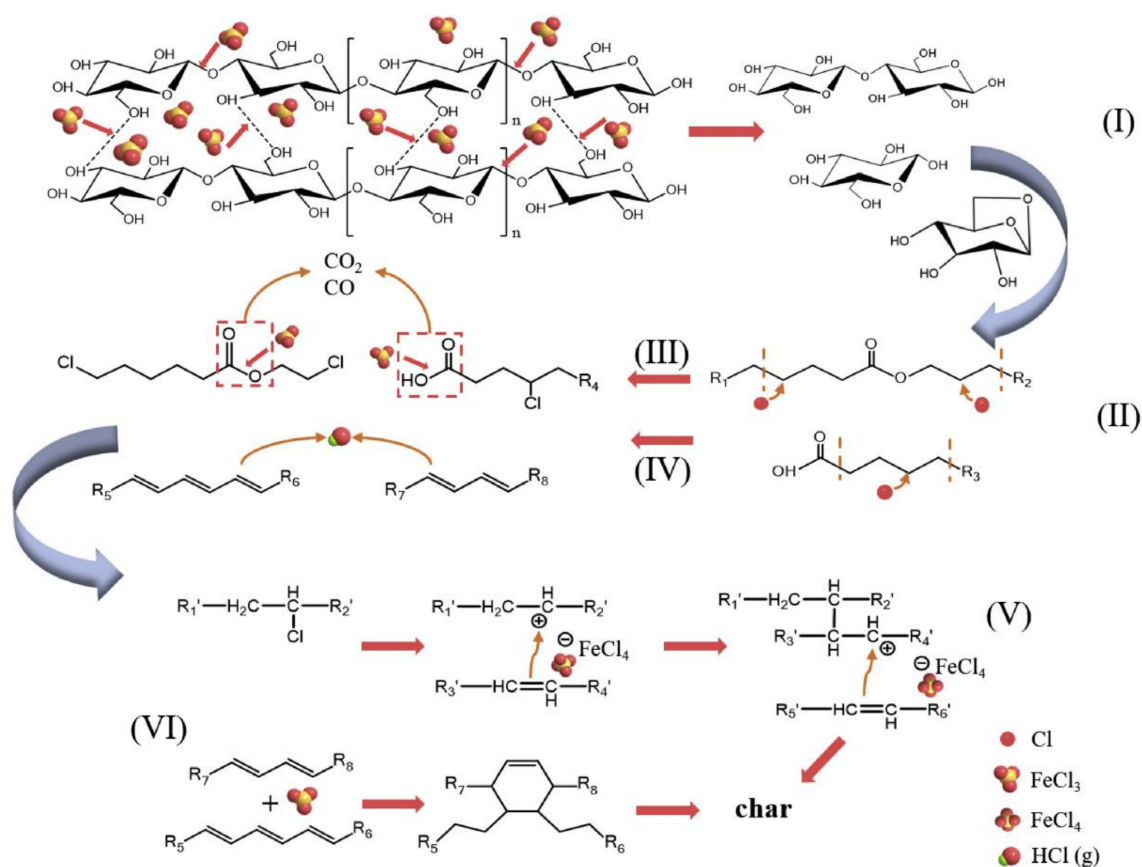


Figure 2. Activation of cotton waste with FeCl_3 (reprinted from [45] with the permission of Elsevier, 2020).

Finally, crosslinking and structure reorganization with transformation of the iron species resulted in the formation of a highly porous activated carbon with highly stable Fe anchored on its surface. Figure 2 schematizes the main reaction occurring during decomposition (I–IV) and char-forming (V–VI) of waste cotton woven with FeCl_3 . At low temperatures ($>100\text{ }^\circ\text{C}$) iron chloride breaks the hydrogen bonds, reducing the polymerization degree of cellulose. Simultaneously, glycoside bonds were also broken by FeCl_3 , generating monosaccharides and disaccharides [53]. Subsequently, as pyrolysis proceeds, (1) cellulose monomers suffer ring opening and chlorine anions (Cl^-) substitute hydrogen atoms, forming chlorine-banded esters (Figure 2, II), and (2) FeCl_3 catalyze decarbonylation and decarboxylation reactions, cracking organic acids and esters into short-chain chlorinated hydrocarbons and releasing CO_2 and CO (Figure 2, III) [53]. Conjugated olefins, which can be considered as a carbon precursor, are produced by dehydrochlorination reaction (Figure 2, IV).

Char formation can proceed through two alternative mechanisms. In the first, the Cl^- of a carbon chain is easily incorporated to FeCl_3 due to its Lewis acid character, and produces FeCl_4^- . Later, carbenium ions are crosslinked with olefins or conjugated unsaturated structures to constitute long organic molecules and more complex carbon structures (Figure 2, V). FeCl_3 , as Lewis acid, catalyzes the hydrogenation and cyclization of the long organic molecules, which constitute the onset of the char formation [54]. The second mechanism, FeCl_3 catalyzes the dechlorination of conjugated olefins by parallel isomerization, aromatization, and cyclization reactions, with the formation of an enriched carbon matrix through inhibition of the tar production (Figure 2, VI) [55].

3. Conditions of Chemical Activation with FeCl₃

As aforementioned, the synthesis procedure of activated carbons by FeCl₃ chemical activation shows three successive steps, namely, (1) impregnation, (2) thermal activation or pyrolysis, and (3) washing. Table 1 summarizes the most relevant activation conditions used for the synthesis of FeCl₃-activated carbons in terms of the technical conditions. Impregnation is the mixture of the carbonaceous precursor with FeCl₃, and it is usually performed by two different methods, in aqueous solution or by physical mixing between the carbon precursor and the iron chloride activating agent. In aqueous solution, the carbonaceous precursor is suspended under stirring in an aqueous solution of FeCl₃, controlling the mass impregnation ratio (R). This parameter is defined as the mass ratio of activating agent to carbon precursor. Usual impregnation mass ratio values are in the range of 0.5:1 up to 5:1. This procedure requires an additional drying step prior to pyrolysis to remove the water. The physical mixing impregnation procedure is simpler since it avoids the drying step, with a consequent cost reduction. This method consists of a mere mixing in the solid state of both the carbonaceous precursor and the iron chloride, in a specific impregnation ratio. In this case, it is advisable to perform a grinding of both materials to assure a better contact among them. The comparison of the characteristics of the activated carbons synthesized using these methods does not draw any clear conclusion. The selection of the mass impregnation ratio is very relevant, as it has shown a very significant effect on the characteristics of the resulting activated carbons, especially in the development of porous texture.

Table 1. Summary of FeCl₃ activation conditions.

Carbon Precursor	Type of Contact	R *	T _{act} * (°C)	t _{act} * (h)	Ref.
Waste cotton	In solution	1.62	400–700	1.0	[44]
Waste cotton	In solution	0.5–2.5	300–800	1.0–2.0	[45]
Lignin	In solution	1.0	500–850	2.0–6.0	[56]
Sewage sludge	In solution	–	750	0.5	[57]
Biomass waste	In solution	–	800	6.0	[58]
Waste cotton	In solution	1.0	400	1.0	[59]
Eucalyptus sawdust	In solution	2.0	700	1.25	[60]
Lotus stem	In solution	4.0	700	1.5	[61]
Sawdust	In solution	0.5–2.0	500–800	1.0	[62]
Coconut shell	In solution	1.0–3.0	700	1.5	[48]
Date pits	In solution	1.5	700	1.0	[63,64]
<i>Arundo donax</i>	In solution	1.65	700	1.0	[65]
Coffee grounds	In solution	1.0	900	1.0	[66]
Coffee husks	In solution	1.0	280	3.0	[67]
Grape seeds	Solid mixing	2.0–4.0	500	2.0	[68]
Chestnut waste	Solid mixing	0.5	220–800	1.0	[69]
Sewage sludge	Solid mixing	0.5–3.0	750	2.0	[70]
Alfalfa leaves	Solid mixing	3.0	900	2.0	[71]
Tara gum	Solid mixing	0.5–3.0	400–1000	2.0	[72]
Lignin	Solid mixing	3.0	800	2.0	[73]
Oily sludge	Solid mixing	1.0–3.0	500–700	1.0	[74]

* R: Impregnation ratio; T_{act}: Activation temperature; t_{act}: Activation time.

The thermal activation step or pyrolysis is the heating of the impregnated mixture under an inert atmosphere (usually N₂) to avoid the oxidation of the carbonaceous matter, from room temperature up to the selected activation temperature (T_{act}). The samples are maintained at the activation temperature during the activation time (t_{act}) and are subsequently cooled down to room temperature under an inert atmosphere. The most relevant parameter of this synthesis stage is without doubt the activation temperature, which controls the extent of the activation mechanism detailed in the previous section. To obtain activated carbons with significant porous development the activation temperature should be equal or higher than 500 °C.

The final washing step is aimed at extracting the remaining activating agent and reaction byproducts to free the newly developed porous texture of the activated carbon. The activated sample is suspended in aqueous acid solutions at temperatures up to 80 °C. Subsequently, the solid activated carbon is filtered and rinsed with plentiful water generally until there is no presence of Cl^- ions or neutral pH in the filtered water. Finally, the activated carbon is dried and ready for use.

Mixtures of Activating Agents

Some studies employed mixtures of iron chloride with other activating agents, even including an activating step in the presence of a gasification agent. In this sense, Guo et al. [75] combined different mixtures of metal activators ($\text{FeCl}_3/\text{MgCl}_2$, $\text{FeCl}_3/\text{ZnCl}_2$, and $\text{ZnCl}_2/\text{MgCl}_2$) under CO_2 to synthesize peanut shell-derived activated carbons used as supercapacitors. This work concludes that FeCl_3 and ZnCl_2 are responsible for microporosity development, while MgCl_2 promotes mesopore formation. Tian et al. [59] also prepared activated carbon by activation of waste cotton with an $\text{FeCl}_3/\text{ZnCl}_2$ mixture. According to this study, the pore development process is due to the creation of molten ZnCl_2 and Fe species, which act as templates to create porosity, and the dehydration effect of ZnCl_2 and FeCl_3 on the carbonaceous cotton waste precursor. Thue et al. [76] prepared activated carbons from wood chips and some inorganic components (lime, ZnCl_2 , and FeCl_3) by microwave heating in very short pyrolysis times (around 11 min). Iron oxide was detected in the synthesized carbons by X-ray diffraction analysis. In another study [77], magnetic activated carbon was obtained by consecutive KOH and FeCl_3 chemical activations. This carbon showed excellent dispersion, easy separation of the aqueous media, and high dye adsorption capacities. Quian et al. [78] analyzed the catalytic effect of different iron salts in the simultaneous magnetization and CO_2 activation of a hydrochar. It was concluded that iron salts had a clear influence on the reaction between the carbon matrix and CO_2 gas, although in the case of iron oxide, the reaction was inhibited by the presence of CO_2 . It was also confirmed that FeCl_3 salt promoted the thermal cracking of the hydrochar, resulting in higher porous development. In contrast, other iron salts ($\text{Fe}_2(\text{SO}_4)_3$, FeC_2O_4 , $\text{Fe}(\text{NO}_3)_3$, and $\text{FeC}_6\text{H}_5\text{O}_7$) do not enhance the porosity due to their inhibition effect on the thermal cracking of hydrochar. Sun et al. [79] used FeCl_3 , MnCl_2 , and AlCl_3 as complementary activating agents in the chemical activation of *Arundo donax* Linn (a perennial grass) with H_3PO_4 under microwave heating. The use of MnCl_2 yielded the activated carbon with the highest porous surface area and pore volume, although the activated carbon prepared using FeCl_3 showed the highest Cr(VI) adsorption capacities. Arroyo-Gómez et al. [80] synthesized activated carbons from peach stones by chemical activation with only ZnCl_2 and a mixture of ZnCl_2 and FeCl_3 (1:1). The study affirmed that the activated carbon obtained with the ZnCl_2 - FeCl_3 mixture showed the highest sensitivity in caffeine detection, probably due to the lower roughness and the presence of mesopores resulting in a better mobility of the caffeine molecules. Activation with ZnCl_2 generally yields activated carbons with a very heterogeneous porous size and the simultaneous presence of both micro- and mesopores. In contrast, as explained in this review (Table 2), FeCl_3 activation yields mainly microporous carbons. Therefore, it is expected that the combination of both activating agents (FeCl_3 and ZnCl_2) produces carbons with intermediate properties. The use of CO_2 gasification in the presence of a melt of FeCl_3 for coal activation has also been analyzed [81]. It was observed that melt infiltration of coal with FeCl_3 resulted in the formation of Fe nanocrystals confined in the inner structure of the coal (Figure 3), which, during the subsequent physical activation with CO_2 , catalyzed the CO_2 gasification of the coal and acted as templates for the formation of the mesoporosity. In the absence of FeCl_3 , the reactivity is much lower, resulting in a lower porosity development. Traditional liquid impregnation with FeCl_3 also improves the reaction of CO_2 and coal, increasing the porosity. However, the presence of iron aggregates, mainly on the external surface of the coal particles, produces a gasification of the external surface with lower porosity development than that of melt infiltration (Figure 3).

Table 2. Characteristic parameters of the porous texture and conditions used to maximize the surface area of activated carbons obtained from different carbon precursors, using FeCl₃ as activating agent.

Carbon Precursor	R	T _{act} (°C)	S _{BET} (m ² ·g ⁻¹)	S _{EXT} (m ² ·g ⁻¹)	V _{mic} (cm ³ ·g ⁻¹)	V _{Total} (cm ³ ·g ⁻¹)	S _{mic} /S _{BET} (%)	Ref.
Waste cotton	1.5	700	942	124	0.33	0.64	87.3	[45]
Lignin	1.0	800	818	31	0.35	0.37	96.2	[56]
Biomass waste	n.p.	800	600	n.p.	n.p.	n.p.	n.p.	[58]
Waste cotton	1.0	400	504	151	0.17	n.p.	72.0	[59]
Eucalyptus sawdust	2.0	700	645	n.p.	0.28	0.44	n.p.	[60]
Lotus stem	4.0	700	374	n.p.	n.p.	0.20	n.p.	[61]
Date pits	1.5	700	780	n.p.	0.47	0.57	n.p.	[63,64]
<i>Arundo donax</i>	1.65	700	927	106	0.36	0.51	88.6	[65]
Coffee grounds	1.0	900	846	n.p.	0.21	n.p.	n.p.	[66]
Coffee husks	1.0	280	965	n.p.	0.53	0.65	n.p.	[67]
Grape seeds	3.0	500	417	54	0.17	0.19	86.8	[68]
Chestnut waste	0.5	800	568	n.p.	n.p.	0.29	n.p.	[69]
Sewage sludge	3.0	750	836	148	0.33	0.62	82.3	[70]
Alfalfa leaves	3.0	900	773	n.p.	n.p.	n.p.	n.p.	[71]
Tara gum	2.0	800	1680	143	0.75	0.99	91.0	[72]
Lignin	3.0	800	951	34	0.44	0.53	96.4	[73]
Oily sludge	2.0	700	683	254	0.20	0.68	62.7	[74]

n.p.: not provided.

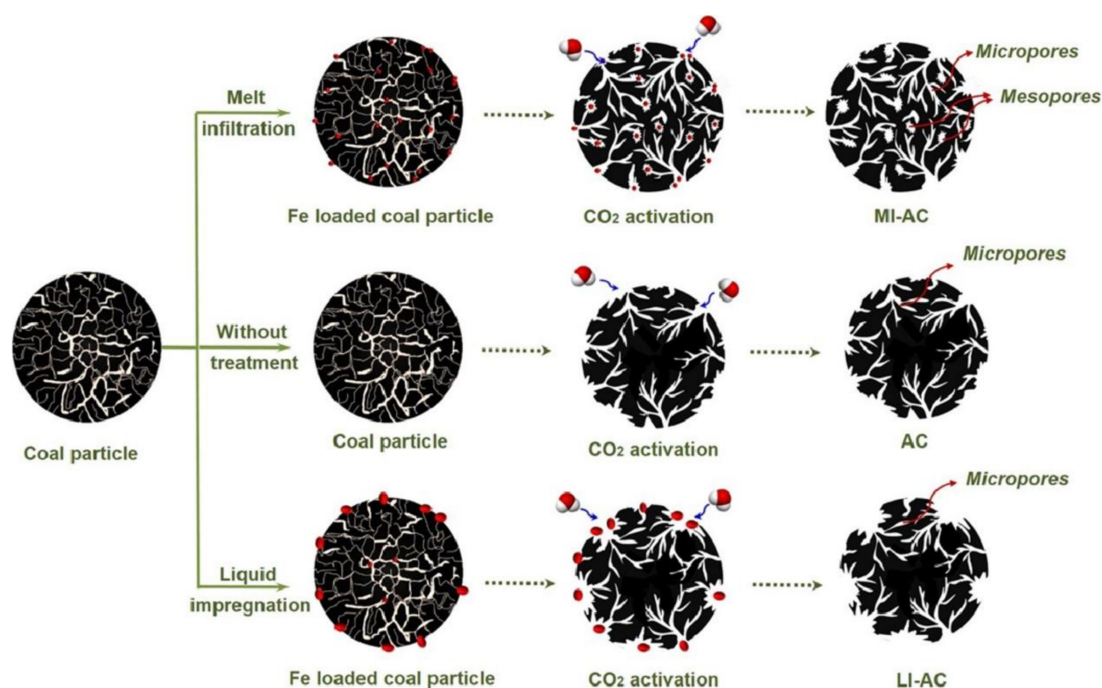


Figure 3. A schematic illustration of the porosity development mechanism by various strategies (reprinted from [81] with the permission of Elsevier, 2018).

4. Characterization of the Activated Carbons

4.1. Porous Texture

The main feature of activated carbons is most probably their well-developed porous texture. Due to this, many of the studies in the literature analyzed the porosity of the carbons obtained by FeCl₃ chemical activation in detail. Table 2 summarizes the characteristic parameters of the porous texture

and the activation conditions used to maximize the total surface area, using FeCl_3 as the activating agent (without the participation of other activation or gasification reagents), where S_{BET} is the total surface area, S_{EXT} the external area, V_{mic} the micropore volume and V_{Total} the total pore volume BET surface areas between 500 and almost 1700 $\text{m}^2\cdot\text{g}^{-1}$ have been reported in the literature, with total pore volumes of almost 1 $\text{cm}^3\cdot\text{g}^{-1}$. The activated carbons prepared through chemical activation with FeCl_3 are essentially microporous, as indicated by the higher percentage values of the $S_{\text{mic}}/S_{\text{BET}}$ parameter. The activation temperatures needed to obtain activated carbons with the most developed porosity, apart from the low values reported by Tian et al. [59] and Oliveira et al. [67], are usually in the range of 700 to 900 °C. Impregnation ratios from 1.0 up to 4.0 were used.

Among the different synthesis parameters, those with more relevance in the final porous texture of the resulting activated carbons are undoubtedly the activation temperature and the impregnation ratio, besides the type of carbon precursor employed. Several works have analyzed the effect of some of these variables in porous texture development. Xu et al. [45] prepared activated carbons from waste cotton woven at different impregnation ratios, activation temperatures, and activation times. It was concluded that activation time has less of an influence on porosity than impregnation ratio and activation temperature. Initially, the increase of the activation time promoted a disordered arrangement. However, a further increase of the activation time resulted in the formation of intermediates that blocked some of the pores and collapsed part of the pore walls. These observations are in agreement with those previously reported by Zazo et al. [56], who obtained activated carbons with surface areas of 791, 818, and 749 $\text{m}^2\cdot\text{g}^{-1}$ when lignin was activated with FeCl_3 at 800 °C for 2, 4, and 6 h, respectively. The effect of the impregnation ratio and the activation temperature was also studied for the FeCl_3 activation of Tara gum and can be observed in Figure 4A,B [72]. The N_2 adsorption–desorption isotherms are characteristic of predominantly microporous materials, although with a contribution of mesoporosity. An initial increase of the impregnation ratio produced an increase of the porosity, as indicated by the higher amount of N_2 adsorbed. However, when the impregnation ratio increased from 2 to 3, a reduction of the amount of N_2 adsorbed is clearly observed (Figure 4A). This reduction can be ascribed to different mechanisms [45]. An excessive amount of FeCl_3 can more intensely catalyze the activation reaction, especially at high activation temperatures, resulting in pore merging and therefore in a reduction of the porosity of the resulting activated carbon [82]. Besides, higher amounts of FeCl_3 can result in larger particles of iron oxides, which can act as a template for the formation of mesopores and/or precipitate in the carbon matrix, altering porous development [83,84]. Similarly, Diaz et al. [68] obtained the maximum surface area at an impregnation ratio equal to 2.0 (in a 1.0–3.0 range) when activating grape seed hydrochars.

The increase of the activation temperature produced activated carbons with more developed porosity. In this sense, Rodríguez-Sánchez et al. [69] observed an increase of the total surface area with activation temperatures in the range of 220 to 800 °C when activating chestnut industrial wastes. However, the use of very high activation temperatures resulted in a lower porosity, as indicated by the lower amount of N_2 adsorbed (mainly in the micropore range, $P/P_0 < 0.4$) when increasing the activation temperature from 800 up to 1000 °C (Figure 4B). This change of trend at the highest activation temperature has different explanations. Boudou et al. [85] affirmed that FeCl_3 is decomposed into iron oxides (Fe_2O_3 and Fe_3O_4), which act as catalysts to gasify the nearest carbon atoms into CH_4 or CO . The porosity reduction is also explained by the shrinkage of the porous texture and the rearrangement of the carbon matrix as a consequence of sintering effects [86]. Finally, Bedia et al. [72] ascribed the decrease in porosity to the increase in the ash content of the carbon with increasing activation temperature. The use of the highest activation temperature resulted in a stronger interaction of the iron with the carbon matrix. This iron is not efficiently extracted during the washing step (indicated by a significant increase in the ash content), blocking part of the porosity.

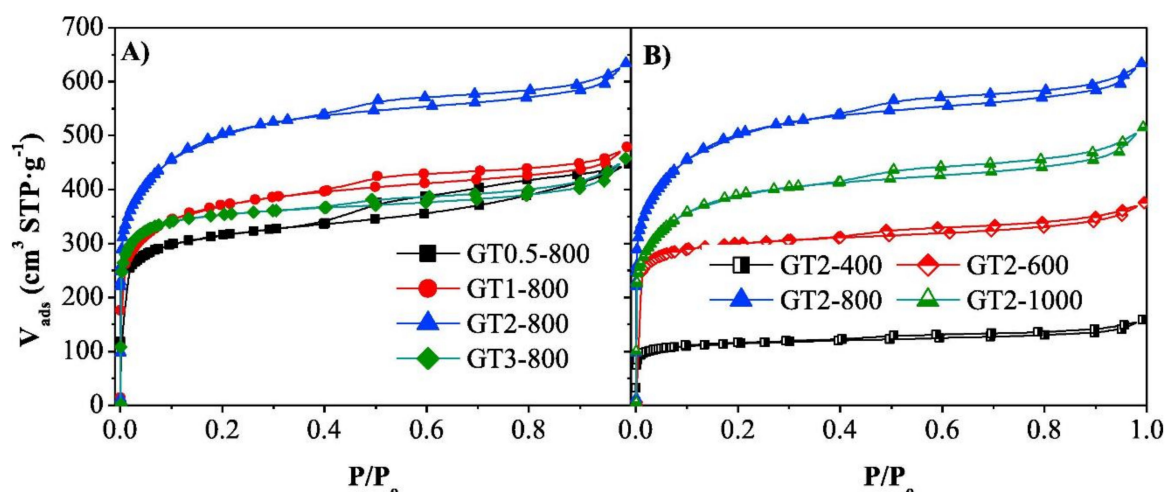


Figure 4. N_2 adsorption–desorption isotherms at $-196\text{ }^\circ\text{C}$ of the activated carbons prepared from Tara gum at (A) different impregnation ratios and $800\text{ }^\circ\text{C}$ and at (B) impregnation ratio of 2 and different activation temperatures (reprinted from [72] with the permission of Elsevier, 2018).

Figure 5 represents the values of the BET surface area of activated carbons synthesized by FeCl_3 of different carbonaceous precursors reported in the literature versus their activation temperatures. As can be seen, there seems to be a clear correlation between porosity development (quantified by the BET surface area) and activation temperature, regardless of other synthesis variables such as impregnation ratio, activation time, or type of carbonaceous precursors. It is also true that some of the values do not fit this general trend. For instance, Oliveira et al. [67] obtained an activated carbon with high porosity from coffee husks at a very low activation temperature of $280\text{ }^\circ\text{C}$. Besides, Bedia et al. [72] synthesized activated carbons with very high values of surface area when using Tara gum as a carbonaceous precursor. In contrast, Mojoudi et al. [74] analyzed the activation of oil sludge. The resulting carbons showed slightly lower surface area values than those observed in the general trend. These divergences are probably due to the effect of the characteristics of the different carbon precursors analyzed in the different studies.

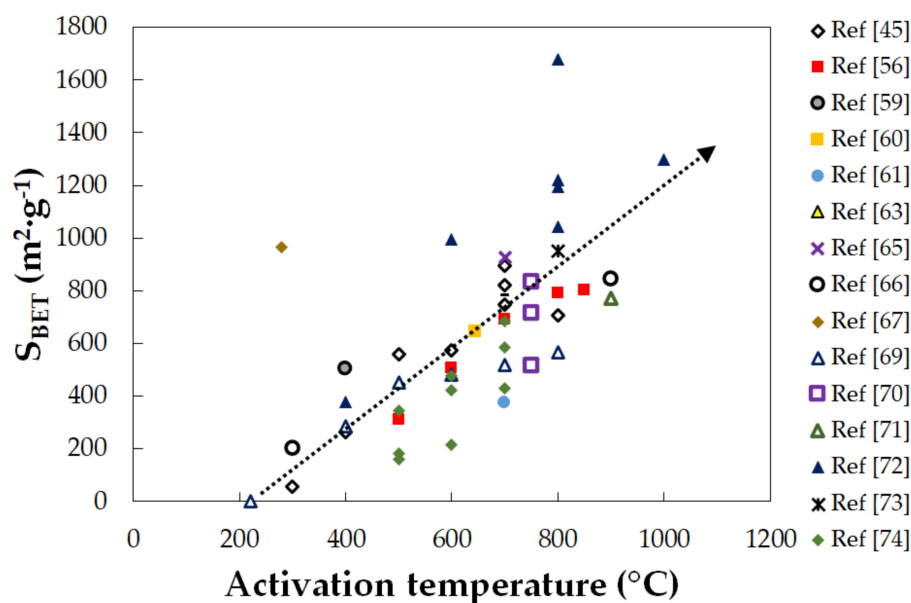


Figure 5. BET surface area of the activated carbons synthesized by FeCl_3 of different carbonaceous precursors versus the activation temperature.

As can be seen, activation with FeCl_3 yields activated carbon with very well-developed porosity and high surface areas up to $1700 \text{ m}^2 \cdot \text{g}^{-1}$. These surface area values are comparable and even higher than those of activated carbons obtained by chemical activation with more traditional activation agents, such as ZnCl_2 or H_3PO_4 . However, the porosity development achieved with FeCl_3 is still far from that obtained when activating with strong bases such as KOH and NaOH .

4.2. Surface Chemistry

FTIR analyses of FeCl_3 -derived activated carbons obtained at different activation temperatures showed a disappearance of the absorption peaks with increasing activation temperatures (Figure 6). The bands at around 3420 cm^{-1} are ascribed to the stretching vibrations of O–H in carbonyl and phenol groups [87]. Conversely, Cazetta et al. [48] affirmed that the FTIR spectra of magnetic activated carbon obtained from biomass waste by FeCl_3 activation did not show bands at these wavelength values, suggesting the absence of hydroxyl groups on these carbons. The authors explained this behavior by the conversion of the surface oxygen groups into iron oxides (magnetite, maghemite, and/or hematite). The other band that remains at an activation temperature of $700 \text{ }^\circ\text{C}$ is located at 1550 cm^{-1} and is related to the C=C stretching vibration in aromatic rings [44,48]. The intensity of this band decreased with increasing activation temperature due to the structure reorganization of the carbon matrix. Finally, the bands located between 1000 and 1300 cm^{-1} are related to the stretching vibration in C–O–C ether bonds. The rest of the bands observed in the sample synthesized at $400 \text{ }^\circ\text{C}$ disappeared when the activation temperature increased. Those at 2520 and 1690 cm^{-1} , related to the stretching vibration of O–H and conjugated stretching vibration of C=O, respectively, disappeared as a consequence of the carbonyl decomposition [88]. Stretching vibrations of aliphatic C–H at 2900 and 1390 cm^{-1} are indicative of an incomplete carbonization of the carbon precursor. Consequently, these bands also disappeared with increasing activation temperature. Finally, low-intensity bands at 735 and 876 cm^{-1} are ascribed to the out-of-plane bending vibrations of aromatic C–H. Other studies reported bands at 557 and 465 cm^{-1} associated to the Fe–O vibrations bonds in Fe_3O_4 [62].

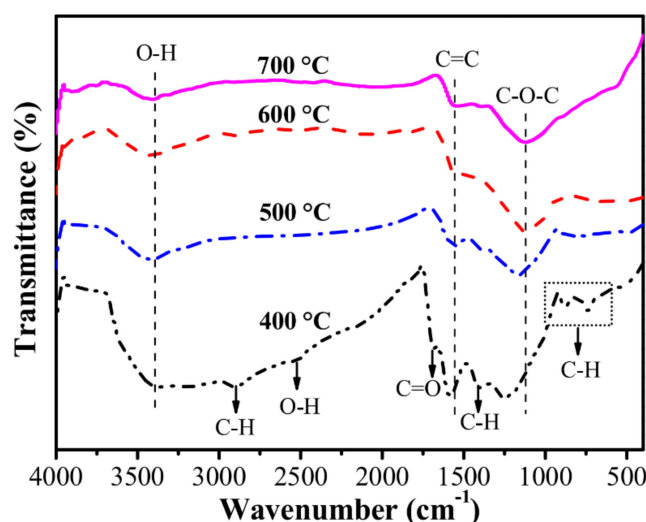


Figure 6. FTIR spectra for activated carbon samples obtained at different pyrolysis temperatures (reprinted from [44] with the permission of Elsevier, 2019).

FTIR analyses suggest the presence of a significant number of acidic surface groups on the activated carbons synthesized by FeCl_3 activation, which was confirmed by measurements of the point of zero charge (pH_{PZC}). In this sense, Tian et al. [59] reported a pH_{PZC} value of 2.41 for an activated carbon obtained from cotton and washed with a 3.2-M solution of HCl . Similar values were obtained also for the activation of cotton waste to prepare an activated carbon washed with a 1-M

HCl aqueous solution [44]. Slightly higher values were obtained by Cazetta et al. [48], who reported pH_{PZC} values of 4.51, 4.12, and 4.10 for magnetic activated carbons synthesized by FeCl_3 activation of coconut shell at impregnation ratios of 1, 2, and 3, respectively. In this latter study, the carbons were submitted to a final washing step with a 1-M HCl aqueous solution. Fu et al. [65] prepared an activated carbon from biomass after washing with a 0.1-M solution of HCl and with a pH_{PZC} of 5.70. The activation of chestnut waste with FeCl_3 at different activation temperatures yielded carbons with surface pH values between 2.3 and 5.2 after washing with distilled water [69]. Our research group synthesized an activated carbon from lignin by FeCl_3 activation using microwave irradiation and a washing step with a 0.1-M aqueous solution of HCl with a pH_{PZC} of 5.0 (results not published). As can be seen, regardless of the conditions of the acid washing step, the activated carbons obtained show predominantly acidic surfaces. This characteristic is particularly relevant when these activated carbons are used as adsorbents.

The analysis of the different XRD results reported in the literature shows some discrepancies between the different studies. Figure 7 represents a standard XRD pattern of an activated carbon (after washing step) obtained through FeCl_3 chemical activation. The broad peaks at around 25 and 43° are the typical characteristic peaks of the (002) and (100) planes of carbon, respectively [89]. The iron-related structures evolve as the carbonization temperature increases. Initially, hydrated iron chloride salts decompose into $\alpha\text{-Fe}_2\text{O}_3$ (hematite) at temperatures of around 400 °C [67,90]. When the carbonization temperature reaches 500 °C, new peaks appear at around 24.3, 33.3, 41.0, 49.6, and 57.7°, corresponding to basal planes (012), (104), (113), (024), and (122) of Fe_3O_4 hematite, respectively. This hematite is formed through the carbothermal reduction of Fe_2O_3 in the presence of the pyrolysis gases and the carbon surface [91]. Some authors affirm that at activation temperatures equal or higher than 700 °C, all the Fe species are reduced to Fe_3O_4 , which confers the magnetic behavior of these carbons [44,60,65,92,93]. In contrast, other studies indicate that at activation temperatures higher than 800 °C, part of the Fe_3O_4 can be transformed into Fe_2C or Fe_3C species due to the interaction with the carbon matrix [62,94].

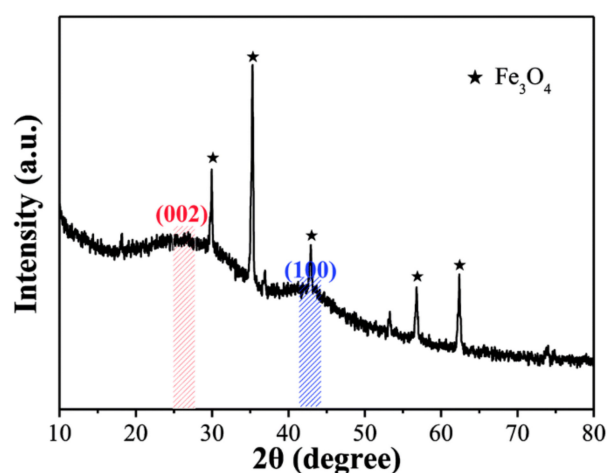


Figure 7. Standard XRD pattern of an activated carbon obtained through FeCl_3 chemical activation at 700 °C (reprinted from [89], RSC, 2018).

XPS analyses have also been extensively employed to characterize the surface chemistry of activated carbons obtained by chemical activation with FeCl_3 . Most of the studies that have used this technique analyzed the Fe2p XPS spectra of the activated carbons in detail. These spectra present a doublet with a separation of 13.6 eV corresponding to $\text{Fe}2\text{p}_{1/2}$ and $\text{Fe}2\text{p}_{3/2}$ signals [95]. Most of the studies agree on the presence of a main band associated to $\text{Fe}2\text{p}_{1/2}$ at approximately 712.0 eV (with a secondary one related to $\text{Fe}2\text{p}_{3/2}$ at around 725.0 eV) and a satellite peak at 718.8 eV, as can be seen in Figure 8 [56,65,70,72]. These peaks are characteristics of Fe^{3+} species, like those in Fe_2O_3 and

partially in Fe_3O_4 as previously observed in XRD patterns. The presence of Fe^0 that is observed at binding energies of around 708.0 eV is discarded [48,96]. Other authors also include a main $\text{Fe}2p_{1/2}$ peak at around 710.2 eV (with its corresponding secondary contribution), ascribed to the presence of Fe^{2+} [44,62] as present in Fe_3O_4 .

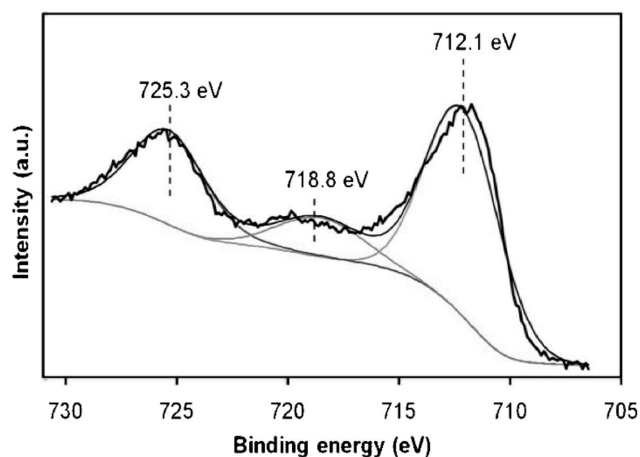


Figure 8. Fe2p XPS spectrum of an activated carbon obtained from lignin by FeCl_3 activation (reprinted from [56] with the permission of Elsevier, 2012).

Some studies have analyzed the iron species by Mössbauer spectroscopy more deeply. Figure 9 represents the room-temperature Mössbauer spectra of activated carbons obtained by chemical activation with FeCl_3 of chestnut industrial waste at different activation temperatures [69]. At the lowest activation temperature, 220 °C, very low absorption is observed because of the low iron concentration. The spectrum shows a single paramagnetic doublet with Mössbauer parameters ($\delta = 0.37 \text{ mms}^{-1}$; $\Delta = 0.85 \text{ mms}^{-1}$), characteristic of Fe^{3+} in a distorted oxygen octahedral coordination. The authors ascribed this behavior to the presence of small-particle Fe^{3+} -containing oxides [97]. At higher activation temperatures (400–600 °C), the spectra show two sextets and a paramagnetic Fe^{3+} doublet. The sextets ($\delta_A = 0.30 \text{ mms}^{-1}$; $2\varepsilon_A = 0.02 \text{ mms}^{-1}$; $H_A = 48.6 \text{ T}$; $\delta_B = 0.66 \text{ mms}^{-1}$; $2\varepsilon_B = -0.01 \text{ mms}^{-1}$; $H_B = 45.2 \text{ T}$) are related to the presence of Fe^{3+} tetrahedral (A) and $\text{Fe}^{2.5+}$ octahedral (B) sites of magnetite (Fe_3O_4) [97]. The doublet is similar to that of the carbon activated at the lowest temperature, and therefore it is also characteristic of superparamagnetic Fe^{3+} oxides. The increase of the activation temperature resulted in more complex Mössbauer spectra. At 700 °C, magnetite and paramagnetic components are also observed, with a new contribution ($\delta = 0.31 \text{ mms}^{-1}$; $2\varepsilon_A = 0.02 \text{ mms}^{-1}$; $H_A = 49.8 \text{ T}$) characteristic of maghemite ($\gamma\text{-Fe}_2\text{O}_3$). Finally, at 800 °C, non-stoichiometric magnetite, maghemite, a small paramagnetic Fe^{3+} contribution, nanophasic iron oxide, metallic iron ($\delta = 0.00 \text{ mms}^{-1}$; $2\varepsilon_A = 0.00 \text{ mms}^{-1}$; $H_A = 33.0 \text{ T}$), and iron carbide cementite (Fe_3C) ($\delta = 0.17 \text{ mms}^{-1}$; $2\varepsilon_A = 0.00 \text{ mms}^{-1}$; $H_A = 20.8 \text{ T}$) were all observed [98].

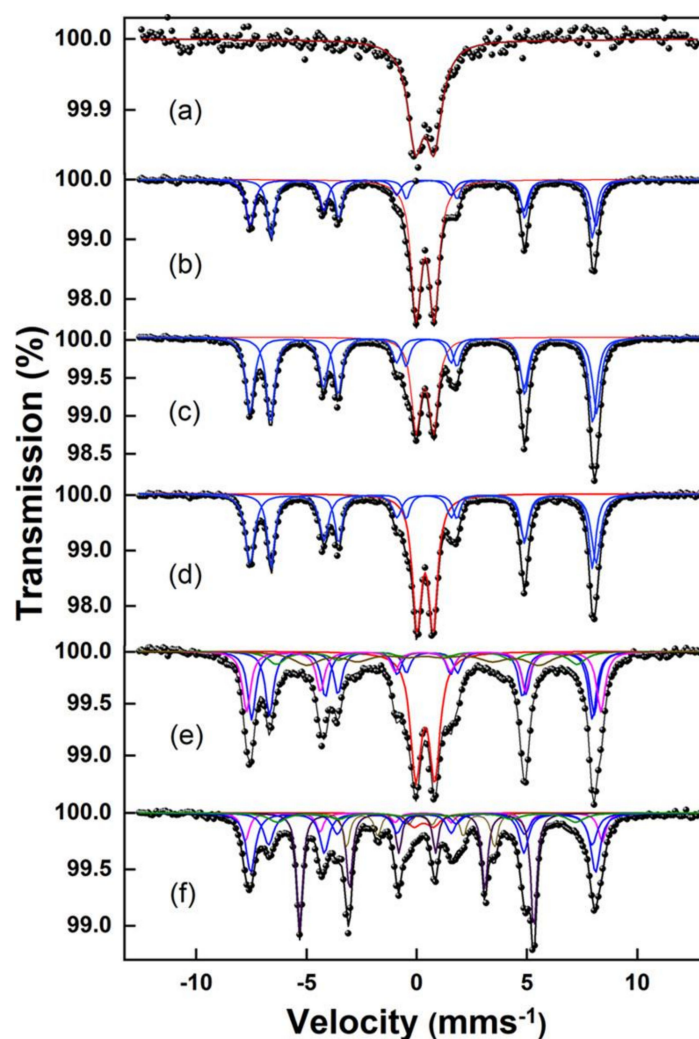


Figure 9. Room-temperature Mössbauer spectra of activated carbons at different activation temperatures (a) 220, (b) 400, (c) 500, (d) 600, (e) 700, and (f) 800 °C (reprinted from [69] with the permission of the ACS, 2019).

4.3. Magnetic Properties

One of the main features of these materials is their magnetism. Magnetic carbons are more suitable for specific applications (e.g., liquid-phase applications) because they are more easily separated from the reaction media using magnets, avoiding the necessity for lengthy centrifugation and/or filtration steps [99–103]. The magnetic properties of FeCl_3 -derived activated carbons have been analyzed using their magnetic hysteresis curves (Figure 10). Those studies showed magnetic hysteresis curves with very low coercivity and almost negligible magnetic hysteresis cycles, characteristic of superparamagnetic materials. Yang et al. [62] reported a maximum specific saturation magnetization close to $60 \text{ emu}\cdot\text{g}^{-1}$ for activated carbons synthesized from sawdust. This study showed an increase of this value with the impregnation ratio (0.5–2.0 range), and a maximum at an activation temperature of 600 °C (in the 500–800 °C interval). Cazetta et al. [48] also observed an increase of the specific saturation magnetization from 17.01 up to $28.74 \text{ emu}\cdot\text{g}^{-1}$ with increasing impregnation ratio from 1 up to 3, respectively. This study shows coercivities in the range of 77–140 Oe and remnant-to-saturation magnetism ratios between 0.11 and 0.21, confirming the superparamagnetic character of the prepared carbons. Chen et al. [60] reported a saturation magnetization value of $30.37 \text{ emu}\cdot\text{g}^{-1}$ with a coercivity force equal to 108.51 Oe and a remnant magnetization of $2.46 \text{ emu}\cdot\text{g}^{-1}$ (remnant-to-saturation magnetism ratio of 0.08). Xu et al. [89] synthesized an activated carbon with $5.2 \text{ emu}\cdot\text{g}^{-1}$ and remanence and coercive forces

equal to $0.30 \text{ emu}\cdot\text{g}^{-1}$ and 63.84 Oe , respectively, confirming the super paramagnetic character of this carbon. It is worth mentioning that these values of specific saturation magnetization are comparable to or higher than others previously reported in the literature for magnetic activated carbon prepared by different synthesis procedures [104–107].

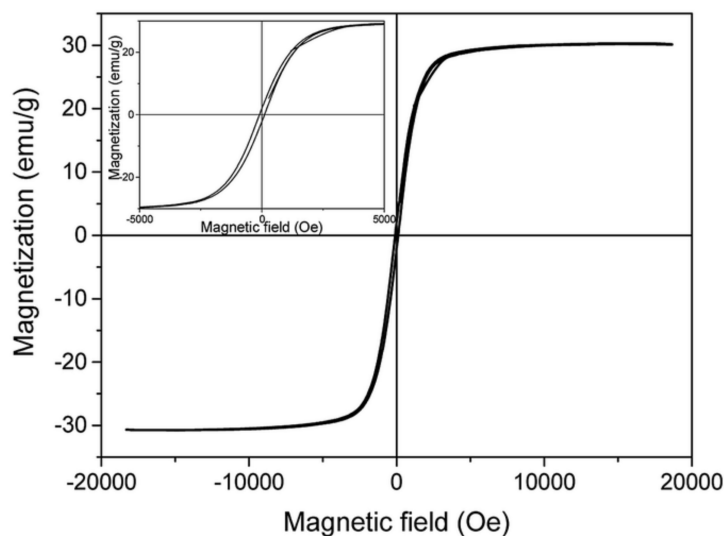


Figure 10. Magnetic hysteresis loop of magnetic activated carbon obtained by FeCl_3 chemical activation (reprinted from [60] with the permission of the RSC, 2019).

5. Applications

5.1. Adsorption

Probably the most well-known application of activated carbons is adsorption, and as a consequence, most of the studies in the literature about FeCl_3 -derived carbons are devoted to adsorption processes, specifically aqueous-phase adsorption processes. This is due to the previously mentioned properties of these activated carbons, namely, well-developed porous texture, surface acidity, and superparamagnetic character. This latter property makes the separation of the activated carbon from the aqueous media using a magnet very simple (Figure 11). Among these studies, adsorption of dyes has attracted much attention, and among the dyes, many studies have analyzed methylene blue (MB) adsorption. This is probably due to the acidic surface of the FeCl_3 -derived carbons (value of the pH_{PZC} lower than or around 5). When the pH of the solution is higher than the pH_{PZC} , the surface of the adsorbent becomes negatively charged, and therefore the positively charged MB molecules ($\text{pK}_a = 0.04$) are more easily attracted to the surface, increasing the adsorption capacity. Chen et al. [60] studied the adsorption of MB on an eucalyptus wood-based FeCl_3 -derived activated carbon. Maximum adsorption capacities of MB between 163 and $192 \text{ mg}\cdot\text{g}^{-1}$ were obtained, increasing the saturation capacity with the adsorption temperature (25 – $55 \text{ }^\circ\text{C}$). The authors concluded that the adsorption process was spontaneous and endothermic, and proceeded through the interaction of the N^+ of the MB molecule and the $-\text{COOH}$ surface groups of the activated carbon. Similarly, Theydan and Ahmed [64] confirmed that the adsorption of MB on activated carbon obtained by chemical activation of date pits with FeCl_3 was also spontaneous and endothermic. They reported a MB saturation adsorption capacity higher than $250 \text{ mg}\cdot\text{g}^{-1}$, in the range of the values obtained when using other types of activated carbons as adsorbents [108–111]. Tian et al. [59] analyzed the adsorption of cationic MB and anionic Eriochrome Black T (EBT) dyes. As expected, the adsorption capacity of MB and EBT followed opposite trends to pH due to the changes in the attraction–repulsion interactions between the dye molecule and the carbon surface. Cazetta et al. [48] analyzed the adsorption of Acid Yellow 6 dye on magnetic activated carbon obtained from coconut shells at different impregnation ratios. The saturation capacity decreased

with increasing pH due to the repulsive interaction between the negatively charged surfaces of the carbon adsorbent ($pH_{PZC} = 4.51$) and the dye molecules at high pH values. Besides the electrostatic interactions, the authors concluded that hydrogen bonding and π - π interactions also have some influence on the adsorption properties. The maximum adsorption capacity was $22.3 \text{ mg}\cdot\text{g}^{-1}$.



Figure 11. Example of adsorption of methylene blue (MB) followed by removal of the magnetic activated carbon with a magnet (adapted from [112]).

Other organic compounds have also been tested in adsorption studies on activated carbons synthesized by chemical activation with FeCl_3 . In this sense, Ahmed and Theydan [63] studied the adsorption of p-nitrophenol on a microporous activated carbon synthesized by FeCl_3 activation of date pits. The adsorption shows an optimum performance at pH equal to 5. At pH values higher than 5, the carbon surface becomes negatively charged, resulting in a decrease of the adsorption capacity due to the electrostatic repulsion with the anionic form of p-nitrophenol molecules ($pK_a = 7.15$) [113]. The maximum adsorption capacity was $185 \text{ mg}\cdot\text{g}^{-1}$, a value comparable to or higher than those obtained with other activated carbon obtained from biomass waste by other activation procedures [114–116]. Mojoudi et al. [74] analyzed the adsorption of phenol and phosphate using activated carbons from oily sludge obtained through physical and chemical activation. The carbon obtained by FeCl_3 activation showed higher adsorption capacities than those physically activated or activated with ZnCl_2 at similar values of surface area. It was suggested that the presence of Fe^{3+} on the carbon surface could be responsible for the high adsorption capacity of phosphate, since Fe^{3+} has a strong affinity for phosphorous species [117]. In the case of phenol, it was adsorbed through π - π interactions between the aromatic structures of the carbon and the aromatic ring of phenol molecule [118]. The maximum phosphate and phenol saturation capacities were 102 and $238 \text{ mg}\cdot\text{g}^{-1}$, respectively. The analysis of the adsorption thermodynamics revealed that the adsorption process is spontaneous and exothermic and proceeds through physisorption.

Several studies have analyzed the adsorption of emerging contaminants on FeCl_3 -derived activated carbons. Fu et al. [65] studied the adsorption of cephalexin antibiotic on activated carbon from *Arundo donax* using different iron salts as activating agents, namely FeCl_3 , FeCl_2 , $\text{FeC}_6\text{H}_5\text{O}_7$, and FeC_2O_4 . The activated carbon obtained by FeCl_3 activation showed the highest adsorption capacity of cephalexin, at $286 \text{ mg}\cdot\text{g}^{-1}$. The work proposed different adsorption mechanisms: (1) Lewis acid–base, (2) electrostatic, and (3) hydrophobic interactions. At the adsorption pH (5.5), the amine group of the cephalexin molecule is protonated and can form a covalent bond with the O of a deprotonated carboxylate surface group of the carbon via Lewis acid–base interaction. Electrostatic interactions can also play a relevant role since at the adsorption pH of 5.5, cephalexin molecules are predominantly in zwitterion form ($pK_{a1} = 2.56$ and $pK_{a2} = 6.88$) and the surface of the carbon is positively charged ($pH_{PZC} = 5.70$). Therefore, electrostatic interactions are expected to play a role in the adsorption

process. Finally, the hydrophobic nature of the surface of the activated carbons can also interact with the hydrophobic molecules of cephalexin. Bedia et al. [72] reported the adsorption of antipyrine, an analgesic, nonsteroidal anti-inflammatory and antipyretic compound, on activated carbons from FeCl₃ activation of Tara gum. The activated carbons were synthesized at different impregnation ratios and activation temperatures. It was concluded that the adsorption capacity is directly related to the values of the total surface area of the carbons, although affected by the presence of oxygen surface groups, which enhanced the adsorption. An antipyrine saturation capacity of 275 mg·g⁻¹ was obtained, a value comparable to or higher than those reported for other emerging contaminants on different activated carbons [119,120]. Diaz et al. [68] analyzed the adsorption of sulfamethoxazole antibiotic on an activated carbon obtained through chemical activation of grape seed hydrochars with different chemical activating agents (KOH, FeCl₃, and ZnCl₂). Although the FeCl₃-derived activated carbon did not achieve the highest adsorption capacity, a significant saturation capacity close to 150 mg·g⁻¹ was reported.

Adsorption of heavy metals from water on FeCl₃-derived carbons has been also analyzed in the literature. Xu et al. [44] analyzed the adsorption of Cr(VI) at an acid pH of 2.0 on FeCl₃-activated carbon from waste cotton textiles. The work concluded that Cr(VI) adsorption proceeds through electrostatic interaction, reduction, and complexation. At the adsorption pH, the mainly negatively charged Cr(VI) species (chromate, CrO₄²⁻, and hydrogen chromate, HCrO₄⁻) have a strong electrostatic attraction through the positively charged surface of the activated carbon (pH_{PZC} = 2.56). Moreover, in the positively charged surface of the carbon adsorbent, the adsorbed Cr(VI) is reduced to Cr(III) by the π electrons of the aromatic rings of the carbon [121,122]. Finally, complexation between Cr(VI) and carboxylate surface groups was also confirmed [123,124]. A similar adsorption mechanism of Cr(VI) was proposed by Feng et al. [61] when analyzing the adsorption on FeCl₃-modified lotus stem-based biochar. Finally, the removal of mercury using a FeCl₃-activated biochar was reported by Yang et al. [62]. The work proposed two active sites for the adsorption/oxidation of Hg⁰, namely Fe³⁺ and oxygen-rich functional groups, especially the C=O groups. Siddique et al. [125] analyzed the adsorption of fluoride anions on an activated carbon obtained by FeCl₃ activation of *Citrus limetta* peels. The maximum adsorption capacity was close to 10 mg·g⁻¹, with the adsorption process being spontaneous and endothermic.

5.2. Catalysis

Fernandez-Ruiz et al. [73] reported the catalytic hydrodechlorination of chloroform on Pd-supported activated carbons obtained by chemical activation of lignin with different activating agents (H₃PO₄, ZnCl₂, FeCl₃, NaOH, and KOH). The aim of the study was to increase the selectivity of the reaction to ethane and propane. While the best results were obtained with NaOH-activated carbon, the surface chemistry of the FeCl₃-derived activated carbon resulted in the smallest mean Pd particle size and the highest metallic-to-electrodeficient Pd ratio, which opens new possibilities for the use of FeCl₃ derived carbon as catalyst or catalytic supports for different applications. Chemical activation with FeCl₃ yielded carbon with (1) a well-developed porous texture, and (2) stable and well-distributed iron species on the carbon surface (Figure 12). Due to these characteristics, several studies [56,57,70] have proposed these types of carbons as catalysts for water purification using catalytic wet peroxide oxidation processes (CWPO). Zazo et al. [56] synthesized highly stable Fe-loaded carbon catalysts by chemical activation of lignin with FeCl₃. One of the main drawbacks of Fe catalysts for CWPO is the iron leaching at the optimal reaction conditions (pH = 3). However, this study reported an almost negligible iron leaching even after 24 h of reaction, as can be seen in Figure 13, confirming the extremely high stability of this type of carbon for this reaction. Bedia et al. [70] synthesized Fe-loaded carbon catalysts by chemical activation of sewage sludge with FeCl₃. They obtained carbon catalysts with well-developed porosity (up to 800 m²·g⁻¹), with iron being stable and homogeneously distributed with Fe particle sizes in the range of 3–11 nm. The most promising sample achieved complete conversion of antipyrine with 70% of mineralization in 1 h at 50 °C. In the field of photocatalysis, activated carbons

are referred to for their use as supports of the active photocatalytic phase to improve the recovery of the photocatalyst from the aqueous medium. Peñas-Garzón et al. [126,127] studied the effect of different activating agents, namely KOH, ZnCl₂, H₃PO₄, and FeCl₃, in the chemical activation of lignin to prepare TiO₂/activated carbon heterostructures. The photocatalyst activated with FeCl₃ (TiO₂/Fe-C) showed the best performance in the photocatalytic treatment of different pharmaceuticals in aqueous solution under solar simulated light, which was attributed to a reduction in the band gap of the TiO₂/Fe-C sample.

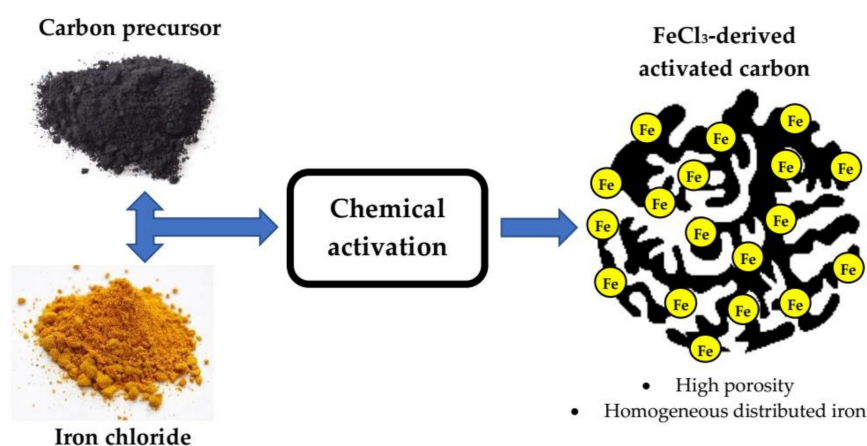


Figure 12. Scheme of FeCl₃ activation and main characteristics of the resulting activated carbons.

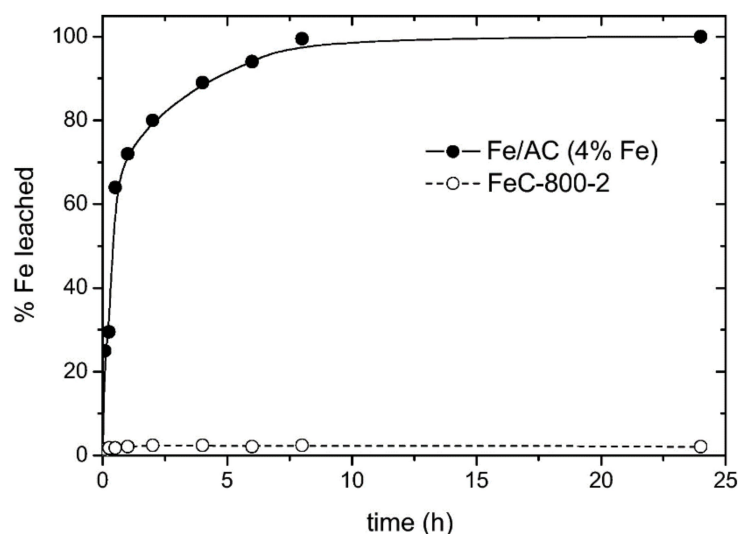


Figure 13. Comparison between the stability of the FeCl₃-derived activated carbon catalyst (FeC-800-2) and activated carbon with iron deposited by the incipient wetness procedure (Fe/AC) (reprinted from [56] with permission of Elsevier, 2012).

5.3. Energy Storage

Batteries and supercapacitors are among the most employed energy storage devices in electronic apparatuses [15,128–130]. The electrodes used in batteries and supercapacitors are continuously being researched, with the aim of improving their performance. Nowadays, most of these electrodes are based on non-renewable carbon sources such as graphite. The search for alternative materials to be used for this application is of great interest. In this sense, Andrijanto et al. [58] analyzed the use of several biomass wastes (corn cob, coconut husk, rice straw, and water hyacinth) as precursors for the synthesis of carbon electrodes using FeCl₃ as an activating agent. The effect of FeCl₃ is twofold, with on one hand the development of the porous texture, and on the other hand the partial graphitization of the carbon

materials, since Fe is a well-known graphitization catalyst [131–135]. FeCl₃ is also responsible for the reduction of carbon resistivity. Finally, Rufford et al. [66] synthesized electrochemical double-layer capacitors (EDLCs) from waste biomass by activation with FeCl₃, MgCl₂, and ZnCl₂. Among them, the FeCl₃-activated carbon supercapacitor prepared at 900 °C showed a specific capacitance of 57 F·g⁻¹, retaining high capacitance value at high current loads. Moreover, the charge-cycling stability of this carbon was excellent.

6. Conclusions and Outlooks

Chemical activation with FeCl₃ has been revealed as a methodology to synthesize activated carbons with interesting properties and promise for different applications such as adsorption, catalysis, and/or energy storage. These carbons are characterized by a well-developed porous texture, composed mainly of micropores. The analysis of the surface chemistry revealed an acidic carbon surface (pH_{PZC} values lower than 5.0), the presence of different oxygen functionalities, and iron species predominantly in the form of Fe³⁺. These iron species are responsible for the superparamagnetic character of these carbons.

Research on this subject should be oriented towards the search for modifications of the synthesis procedure, an analysis of new carbon precursors, and the tailoring of the porosity and iron content of the final carbons. On this basis, the future applications of these carbons will be expanded, opening up new possibilities. Adsorption processes can be improved using well-developed porosity, a main composition of micropores, and surface chemistry of an acid nature for these types of activated carbons, making them ideal adsorbents for the removal and purification of both liquid and gas streams. Moreover, their super paramagnetic character facilitates their separation from the liquid media, which constitutes an enormous advantage in relation to other activated carbons or adsorbents. FeCl₃-activated carbons are also promising candidates for catalytic applications, and as supports or as mass catalysts. The presence of well-distributed iron particles on the well-developed surface, as well as the high stability of Fe (which seems to be intimately attached in the carbon matrix during the synthesis stage), make these carbons promising materials for different catalytic applications. Some studies have already probed their high activity and stability in different catalytic reactions. Their use for energy storage applications is also favored by well-developed porosity and the presence of iron, which seem to produce a limited graphitization of the carbon structure and enhance carbon conductivity. Finally, researchers must find procedures for implementing these materials at the industrial scale, taking into account other aspects not yet analyzed such as the cost of the overall manufacturing process.

Author Contributions: J.B., M.P.-G., A.G.-A., J.J.R., and C.B. wrote and revised the manuscript. All authors have read and agreed to the published version of the manuscript.

Funding: This research was funded by Spanish MINECO project CTQ2016–78576-R.

Acknowledgments: The authors acknowledge financial support from the Spanish MINECO (project CTQ2016–78576-R). M. Peñas-Garzón is indebted to the Spanish MECO for the FPU16/00576 predoctoral contract.

Conflicts of Interest: The authors declare no conflict of interest.

References

1. Marsh, H.; Rodríguez-Reinoso, F. *Activated Carbon*; Elsevier Ltd.: Amsterdam, The Netherlands, 2006; ISBN 9780080444635.
2. Çeçen, F.; Aktaş, Ö. *Activated Carbon for Water and Wastewater Treatment: Integration of Adsorption and Biological Treatment*; Wiley-VCH: Weinheim, Germany, 2011; ISBN 9783527324712.
3. Bansal, R.C.; Goyal, M. *Activated Carbon Adsorption*; CRC Press: Boca Raton, FL, USA, 2005; ISBN 9781420028812.
4. Rouquerol, J.; Rouquerol, F.; Llewellyn, P.; Maurin, G.; Sing, K.S.W. *Adsorption by Powders and Porous Solids: Principles, Methodology and Applications*, 2nd ed.; Elsevier Inc.: Amsterdam, The Netherlands, 2013; ISBN 9780080970356.

5. Bedia, J.; Rosas, J.M.; Rodríguez-Mirasol, J.; Cordero, T. Pd supported on mesoporous activated carbons with high oxidation resistance as catalysts for toluene oxidation. *Appl. Catal. B Environ.* **2010**, *94*, 8–18. [[CrossRef](#)]
6. Martín-Martínez, M.; Gómez-Sainero, L.M.; Álvarez-Montero, M.A.; Bedia, J.; Rodríguez, J.J. Comparison of different precious metals in activated carbon-supported catalysts for the gas-phase hydrodechlorination of chloromethanes. *Appl. Catal. B Environ.* **2013**, *132–133*, 256–265. [[CrossRef](#)]
7. Palomo, J.; Rodríguez-Cano, M.A.; Rodríguez-Mirasol, J.; Cordero, T. On the kinetics of methanol dehydration to dimethyl ether on Zr-loaded P-containing mesoporous activated carbon catalyst. *Chem. Eng. J.* **2019**, *378*, 122198. [[CrossRef](#)]
8. Fang, R.; Huang, H.; Ji, J.; He, M.; Feng, Q.; Zhan, Y.; Leung, D.Y.C. Efficient MnOx supported on coconut shell activated carbon for catalytic oxidation of indoor formaldehyde at room temperature. *Chem. Eng. J.* **2018**, *334*, 2050–2057. [[CrossRef](#)]
9. Rey, A.; Hungria, A.B.; Duran-Valle, C.J.; Faraldos, M.; Bahamonde, A.; Casas, J.A.; Rodríguez, J.J. On the optimization of activated carbon-supported iron catalysts in catalytic wet peroxide oxidation process. *Appl. Catal. B Environ.* **2016**, *181*, 249–259. [[CrossRef](#)]
10. Bedia, J.; Ruiz-Rosas, R.; Rodríguez-Mirasol, J.; Cordero, T. Kinetic study of the decomposition of 2-butanol on carbon-based acid catalyst. *AIChE J.* **2010**, *56*, 1557–1568. [[CrossRef](#)]
11. Cordero, T.; Rodríguez-Mirasol, J.; Bedia, J.; Gomis, S.; Yustos, P.; García-Ochoa, F.; Santos, A. Activated carbon as catalyst in wet oxidation of phenol: Effect of the oxidation reaction on the catalyst properties and stability. *Appl. Catal. B Environ.* **2008**, *81*, 122–131. [[CrossRef](#)]
12. Valero-Romero, M.J.; Calvo-Muñoz, E.M.; Ruiz-Rosas, R.; Rodríguez-Mirasol, J.; Cordero, T. Phosphorus-Containing Mesoporous Carbon Acid Catalyst for Methanol Dehydration to Dimethyl Ether. *Ind. Eng. Chem. Res.* **2019**, *58*, 4042–4053. [[CrossRef](#)]
13. Rey, A.; Faraldos, M.; Bahamonde, A.; Casas, J.A.; Zazo, J.A.; Rodríguez, J.J. Role of the Activated Carbon Surface on Catalytic Wet Peroxide Oxidation. *Ind. Eng. Chem. Res.* **2008**, *47*, 8166–8174. [[CrossRef](#)]
14. Shi, H. Activated carbons and double layer capacitance. *Electrochim. Acta* **1996**, *41*, 1633–1639. [[CrossRef](#)]
15. Qu, D. Studies of the activated carbons used in double-layer supercapacitors. *J. Power Sources* **2002**, *109*, 403–411. [[CrossRef](#)]
16. Wei, L.; Yushin, G. Nanostructured activated carbons from natural precursors for electrical double layer capacitors. *Nano Energy* **2012**, *1*, 552–565. [[CrossRef](#)]
17. Abioye, A.M.; Ani, F.N. Recent development in the production of activated carbon electrodes from agricultural waste biomass for supercapacitors: A review. *Renew. Sustain. Energy Rev.* **2015**, *52*, 1282–1293. [[CrossRef](#)]
18. Ibeh, P.O.; García-Mateos, F.J.; Rosas, J.M.; Rodríguez-Mirasol, J.; Cordero, T. Activated carbon monoliths from lignocellulosic biomass waste for electrochemical applications. *J. Taiwan Inst. Chem. Eng.* **2019**, *97*, 480–488. [[CrossRef](#)]
19. Rodríguez, J.J.; Cordero, T.; Rodríguez-Mirasol, J. Carbon Materials from Lignin and Their Applications. In *Production of Biofuels and Chemicals from Lignin*; Springer: Berlin/Heidelberg, Germany, 2016; pp. 217–262. ISBN 978-981-10-1964-7.
20. Pui, W.K.; Yusoff, R.; Aroua, M.K. A review on activated carbon adsorption for volatile organic compounds (VOCs). *Rev. Chem. Eng.* **2019**, *35*, 649–668. [[CrossRef](#)]
21. Kosheleva, R.I.; Mitropoulos, A.C.; Kyzas, G.Z. Synthesis of activated carbon from food waste. *Environ. Chem. Lett.* **2019**, *17*, 429–438. [[CrossRef](#)]
22. Bedia, J.; Peñas-Garzón, M.; Gómez-Avilés, A.; Rodríguez, J.; Bolver, C. A Review on the Synthesis and Characterization of Biomass-Derived Carbons for Adsorption of Emerging Contaminants from Water. *C. J. Carbon Res.* **2018**, *4*, 63. [[CrossRef](#)]
23. Völker, J.; Stapf, M.; Miehe, U.; Wagner, M. Systematic Review of Toxicity Removal by Advanced Wastewater Treatment Technologies via Ozonation and Activated Carbon. *Environ. Sci. Technol.* **2019**, *53*, 7215–7233. [[CrossRef](#)]
24. Lakshmi, S.D.; Avti, P.K.; Hegde, G. Activated carbon nanoparticles from biowaste as new generation antimicrobial agents: A review. *Nano-Struct. Nano-Objects* **2018**, *16*, 306–321. [[CrossRef](#)]
25. Labus, K.; Gryglewicz, S.; Machnikowski, J. Granular KOH-activated carbons from coal-based cokes and their CO₂ adsorption capacity. *Fuel* **2014**, *118*, 9–15. [[CrossRef](#)]
26. Chingombe, P.; Saha, B.; Wakeman, R.J. Surface modification and characterisation of a coal-based activated carbon. *Carbon N. Y.* **2005**, *43*, 3132–3143. [[CrossRef](#)]

27. Bagreev, A.; Menendez, J.A.; Dukhno, I.; Tarasenko, Y.; Bandosz, T.J. Bituminous coal-based activated carbons modified with nitrogen as adsorbents of hydrogen sulfide. *Carbon N. Y.* **2004**, *42*, 469–476. [[CrossRef](#)]
28. Acevedo, B.; Barriocanal, C.; Lupul, I.; Gryglewicz, G. Properties and performance of mesoporous activated carbons from scrap tyres, bituminous wastes and coal. *Fuel* **2015**, *151*, 83–90. [[CrossRef](#)]
29. Gupta, V.K.; Nayak, A.; Agarwal, S.; Tyagi, I. Potential of activated carbon from waste rubber tire for the adsorption of phenolics: Effect of pre-treatment conditions. *J. Colloid Interface Sci.* **2014**, *417*, 420–430. [[CrossRef](#)]
30. Ramírez-Arias, A.M.; Moreno-Piraján, J.C.; Giraldo, L. Adsorption of Triton X-100 in aqueous solution on activated carbon obtained from waste tires for wastewater decontamination. *Adsorption* **2020**, *26*, 303–316. [[CrossRef](#)]
31. Rosas, J.M.; Ruiz-Rosas, R.; Rodríguez-Mirasol, J.; Cordero, T. Kinetic study of SO₂ removal over lignin-based activated carbon. *Chem. Eng. J.* **2017**, *307*, 707–721. [[CrossRef](#)]
32. Cotoruelo, L.M.; Marqués, M.D.; Díaz, F.J.; Rodríguez-Mirasol, J.; Rodríguez, J.J.; Cordero, T. Adsorbent ability of lignin-based activated carbons for the removal of p-nitrophenol from aqueous solutions. *Chem. Eng. J.* **2012**, *184*, 176–183. [[CrossRef](#)]
33. Rodríguez-Mirasol, J.; Bedia, J.; Cordero, T.; Rodríguez, J. Influence of water vapor on the adsorption of VOCs on lignin-based activated carbons. *Sep. Sci. Technol.* **2005**, *40*, 3113–3135. [[CrossRef](#)]
34. Shen, Y.; Zhou, Y.; Fu, Y.; Zhang, N. Activated carbons synthesized from unaltered and pelletized biomass wastes for bio-tar adsorption in different phases. *Renew. Energy* **2020**, *146*, 1700–1709. [[CrossRef](#)]
35. Liou, T.H. Development of mesoporous structure and high adsorption capacity of biomass-based activated carbon by phosphoric acid and zinc chloride activation. *Chem. Eng. J.* **2010**, *158*, 129–142. [[CrossRef](#)]
36. Rosas, J.M.; Bedia, J.; Rodríguez-Mirasol, J.; Cordero, T. Preparation of Hemp-Derived Activated Carbon Monoliths. Adsorption of Water Vapor. *Ind. Eng. Chem. Res.* **2008**, *47*, 1288–1296. [[CrossRef](#)]
37. Saleem, J.; Shahid, U.B.; Hijab, M.; Mackey, H.; McKay, G. Production and applications of activated carbons as adsorbents from olive stones. *Biomass Convers. Biorefinery* **2019**, *9*, 775–802. [[CrossRef](#)]
38. Ioannidou, O.; Zabaniotou, A. Agricultural residues as precursors for activated carbon production—A review. *Renew. Sustain. Energy Rev.* **2007**, *11*, 1966–2005. [[CrossRef](#)]
39. Dias, J.M.; Alvim-Ferraz, M.C.M.; Almeida, M.F.; Rivera-Utrilla, J.; Sánchez-Polo, M. Waste materials for activated carbon preparation and its use in aqueous-phase treatment: A review. *J. Environ. Manag.* **2007**, *85*, 833–846. [[CrossRef](#)]
40. Ye, N.; Wang, Z.; Wang, S.; Peijnenburg, W.J.G.M. Toxicity of mixtures of zinc oxide and graphene oxide nanoparticles to aquatic organisms of different trophic level: Particles outperform dissolved ions. *Nanotoxicology* **2018**, *12*, 423–438. [[CrossRef](#)]
41. Holmes, A.M.; Mackenzie, L.; Roberts, M.S. Disposition and measured toxicity of zinc oxide nanoparticles and zinc ions against keratinocytes in cell culture and viable human epidermis. *Nanotoxicology* **2020**, *14*, 263–274. [[CrossRef](#)]
42. Demarchi, C.A.; Michel, B.S.; Nedelko, N.; Ślawska-Waniewska, A.; Dłużewski, P.; Kaleta, A.; Minikayev, R.; Strachowski, T.; Lipińska, L.; Dal Magro, J.; et al. Preparation, characterization, and application of magnetic activated carbon from termite feces for the adsorption of Cr(VI) from aqueous solutions. *Powder Technol.* **2019**, *354*, 432–441. [[CrossRef](#)]
43. Cesano, F.; Cravanzola, S.; Brunella, V.; Damin, A.; Scarano, D. From Polymer to Magnetic Porous Carbon Spheres: Combined Microscopy, Spectroscopy, and Porosity Studies. *Front. Mater.* **2019**, *6*, 84. [[CrossRef](#)]
44. Xu, Z.; Sun, Z.; Zhou, Y.; Chen, W.; Zhang, T.; Huang, Y.; Zhang, D. Insights into the pyrolysis behavior and adsorption properties of activated carbon from waste cotton textiles by FeCl₃-activation. *Colloids Surf. A Physicochem. Eng. Asp.* **2019**, *582*, 123934. [[CrossRef](#)]
45. Xu, Z.; Zhou, Y.; Sun, Z.; Zhang, D.; Huang, Y.; Gu, S.; Chen, W. Understanding reactions and pore-forming mechanisms between waste cotton woven and FeCl₃ during the synthesis of magnetic activated carbon. *Chemosphere* **2020**, *241*, 125120. [[CrossRef](#)]
46. Zhu, X.; Qian, F.; Liu, Y.; Matera, D.; Wu, G.; Zhang, S.; Chen, J. Controllable synthesis of magnetic carbon composites with high porosity and strong acid resistance from hydrochar for efficient removal of organic pollutants: An overlooked influence. *Carbon N. Y.* **2016**, *99*, 338–347. [[CrossRef](#)]
47. Vinu, R.; Broadbelt, L.J. A mechanistic model of fast pyrolysis of glucose-based carbohydrates to predict bio-oil composition. *Energy Environ. Sci.* **2012**, *5*, 9808–9826. [[CrossRef](#)]

48. Cazetta, A.L.; Pezoti, O.; Bedin, K.C.; Silva, T.L.; Paesano Junior, A.; Asefa, T.; Almeida, V.C. Magnetic Activated Carbon Derived from Biomass Waste by Concurrent Synthesis: Efficient Adsorbent for Toxic Dyes. *ACS Sustain. Chem. Eng.* **2016**, *4*, 1058–1068. [[CrossRef](#)]
49. Gong, X.; Guo, Z.; Wang, Z. Variation of char structure during anthracite pyrolysis catalyzed by Fe₂O₃ and its influence on char combustion reactivity. *Energy Fuels* **2009**, *23*, 4547–4552. [[CrossRef](#)]
50. Falco, C.; Baccile, N.; Titirici, M.M. Morphological and structural differences between glucose, cellulose and lignocellulosic biomass derived hydrothermal carbons. *Green Chem.* **2011**, *13*, 3273–3281. [[CrossRef](#)]
51. Falco, C.; Perez Caballero, F.; Babonneau, F.; Gervais, C.; Laurent, G.; Titirici, M.M.; Baccile, N. Hydrothermal carbon from biomass: Structural differences between hydrothermal and pyrolyzed carbons via ¹³C solid state NMR. *Langmuir* **2011**, *27*, 14460–14471. [[CrossRef](#)] [[PubMed](#)]
52. Zhu, X.; Liu, Y.; Luo, G.; Qian, F.; Zhang, S.; Chen, J. Facile fabrication of magnetic carbon composites from hydrochar via simultaneous activation and magnetization for triclosan adsorption. *Environ. Sci. Technol.* **2014**, *48*, 5840–5848. [[CrossRef](#)]
53. Yang, X.; Zhao, Y.; Li, R.; Wu, Y.; Yang, M. A modified kinetic analysis method of cellulose pyrolysis based on TG–FTIR technique. *Thermochim. Acta* **2018**, *665*, 20–27. [[CrossRef](#)]
54. Stoeva, S.; Karaivanova, M.; Benev, D. Poly(vinyl chloride) composition. II. Study of the flammability and smoke-evolution of unplasticized poly(vinyl chloride) and fire-retardant additives. *J. Appl. Polym. Sci.* **1992**, *46*, 119–127. [[CrossRef](#)]
55. Chen, Y.; Zhang, S.; Han, X.; Zhang, X.; Yi, M.; Yang, S.; Yu, D.; Liu, W. Catalytic Dechlorination and Charring Reaction of Polyvinyl Chloride by CuAl Layered Double Hydroxide. *Energy Fuels* **2018**, *32*, 2407–2413. [[CrossRef](#)]
56. Zazo, J.A.; Bedia, J.; Fierro, C.M.; Pliego, G.; Casas, J.A.; Rodriguez, J.J. Highly stable Fe on activated carbon catalysts for CWPO upon FeCl₃ activation of lignin from black liquors. *Catal. Today* **2012**, *187*, 115–121. [[CrossRef](#)]
57. Mohedano, A.F.; Monsalvo, V.M.; Bedia, J.; Lopez, J.; Rodriguez, J.J. Highly stable iron catalysts from sewage sludge for CWPO. *J. Environ. Chem. Eng.* **2014**, *2*, 2359–2364. [[CrossRef](#)]
58. Andrijanto, E.; Purwaningsih, I.; Silvia, L.; Subiyanto, G.; Hulupi, M. The conversion of biomass into carbon electrode material using FeCl₃ as an activating agent for battery application. In *IOP Conference Series: Earth and Environmental Science*; Institute of Physics Publishing: Bristol, UK, 2019; Volume 299, p. 012001.
59. Tian, D.; Xu, Z.; Zhang, D.; Chen, W.; Cai, J.; Deng, H.; Sun, Z.; Zhou, Y. Micro–mesoporous carbon from cotton waste activated by FeCl₃/ZnCl₂: Preparation, optimization, characterization and adsorption of methylene blue and eriochrome black T. *J. Solid State Chem.* **2019**, *269*, 580–587. [[CrossRef](#)]
60. Chen, C.; Mi, S.; Lao, D.; Shi, P.; Tong, Z.; Li, Z.; Hu, H. Single-step synthesis of eucalyptus sawdust magnetic activated carbon and its adsorption behavior for methylene blue. *RSC Adv.* **2019**, *9*, 22248–22262. [[CrossRef](#)]
61. Feng, Z.; Chen, N.; Feng, C.; Gao, Y. Mechanisms of Cr(VI) removal by FeCl₃-modified lotus stem-based biochar (FeCl₃@LS-BC) using mass-balance and functional group expressions. *Colloids Surf. A Physicochem. Eng. Asp.* **2018**, *551*, 17–24. [[CrossRef](#)]
62. Yang, J.; Zhao, Y.; Ma, S.; Zhu, B.; Zhang, J.; Zheng, C. Mercury Removal by Magnetic Biochar Derived from Simultaneous Activation and Magnetization of Sawdust. *Environ. Sci. Technol.* **2016**, *50*, 12040–12047. [[CrossRef](#)]
63. Ahmed, M.J.; Theydan, S.K. Adsorptive removal of p-nitrophenol on microporous activated carbon by FeCl₃ activation: Equilibrium and kinetics studies. *Desalin. Water Treat.* **2015**, *55*, 522–531. [[CrossRef](#)]
64. Theydan, S.K.; Ahmed, M.J. Adsorption of methylene blue onto biomass-based activated carbon by FeCl₃ activation: Equilibrium, kinetics, and thermodynamic studies. *J. Anal. Appl. Pyrolysis* **2012**, *97*, 116–122. [[CrossRef](#)]
65. Fu, K.; Yue, Q.; Gao, B.; Sun, Y.; Wang, Y.; Li, Q.; Zhao, P.; Chen, S. Physicochemical and adsorptive properties of activated carbons from *Arundo donax* Linn utilizing different iron salts as activating agents. *J. Taiwan Inst. Chem. Eng.* **2014**, *45*, 3007–3015. [[CrossRef](#)]
66. Rufford, T.E.; Hulicova-Jurcakova, D.; Zhu, Z.; Lu, G.Q. A comparative study of chemical treatment by FeCl₃, MgCl₂, and ZnCl₂ on microstructure, surface chemistry, and double-layer capacitance of carbons from waste biomass. *J. Mater. Res.* **2010**, *25*, 1451–1459. [[CrossRef](#)]

67. Oliveira, L.C.A.; Pereira, E.; Guimaraes, I.R.; Vallone, A.; Pereira, M.; Mesquita, J.P.; Sapag, K. Preparation of activated carbons from coffee husks utilizing FeCl₃ and ZnCl₂ as activating agents. *J. Hazard. Mater.* **2009**, *165*, 87–94. [[CrossRef](#)] [[PubMed](#)]
68. Diaz, E.; Manzano, F.J.; Villamil, J.; Rodriguez, J.J.; Mohedano, A.F. Low-Cost Activated Grape Seed-Derived Hydrochar through Hydrothermal Carbonization and Chemical Activation for Sulfamethoxazole Adsorption. *Appl. Sci.* **2019**, *9*, 5127. [[CrossRef](#)]
69. Rodríguez-Sánchez, S.; Ruiz, B.; Martínez-Blanco, D.; Sánchez-Arenillas, M.; Diez, M.A.; Suárez-Ruiz, I.; Marco, J.F.; Blanco, J.; Fuente, E. Sustainable Thermochemical Single-Step Process to Obtain Magnetic Activated Carbons from Chestnut Industrial Wastes. *ACS Sustain. Chem. Eng.* **2019**, *7*, 17293–17305. [[CrossRef](#)]
70. Bedia, J.; Monsalvo, V.M.; Rodriguez, J.J.; Mohedano, A.F. Iron catalysts by chemical activation of sewage sludge with FeCl₃ for CWPO. *Chem. Eng. J.* **2017**, *318*, 224–230. [[CrossRef](#)]
71. Deng, L.; Yuan, Y.; Zhang, Y.; Wang, Y.; Chen, Y.; Yuan, H.; Chen, Y. Alfalfa Leaf-Derived Porous Heteroatom-Doped Carbon Materials as Efficient Cathodic Catalysts in Microbial Fuel Cells. *ACS Sustain. Chem. Eng.* **2017**, *5*, 9766–9773. [[CrossRef](#)]
72. Bedia, J.; Belver, C.; Ponce, S.; Rodriguez, J.; Rodriguez, J.J. Adsorption of antipyrine by activated carbons from FeCl₃-activation of Tara gum. *Chem. Eng. J.* **2018**, *333*, 58–65. [[CrossRef](#)]
73. Fernandez-Ruiz, C.; Bedia, J.; Bonal, P.; Rodriguez, J.J.; Gómez-Sainero, L.M. Chloroform conversion into ethane and propane by catalytic hydrodechlorination with Pd supported on activated carbons from lignin. *Catal. Sci. Technol.* **2018**, *8*, 3926–3935. [[CrossRef](#)]
74. Mojoudi, N.; Soleimani, M.; Mirghaffari, N.; Belver, C.; Bedia, J. Removal of phenol and phosphate from aqueous solutions using activated carbons prepared from oily sludge through physical and chemical activation. *Water Sci. Technol.* **2019**, *80*, 575–586. [[CrossRef](#)] [[PubMed](#)]
75. Guo, F.; Jiang, X.; Jia, X.; Liang, S.; Qian, L.; Rao, Z. Synthesis of biomass carbon electrode materials by bimetallic activation for the application in supercapacitors. *J. Electroanal. Chem.* **2019**, *844*, 105–115. [[CrossRef](#)]
76. Thue, P.S.; Adebayo, M.A.; Lima, E.C.; Sieliechi, J.M.; Machado, F.M.; Dotto, G.L.; Vaghetti, J.C.P.; Dias, S.L.P. Preparation, characterization and application of microwave-assisted activated carbons from wood chips for removal of phenol from aqueous solution. *J. Mol. Liq.* **2016**, *223*, 1067–1080. [[CrossRef](#)]
77. Gao, X.; Zhang, Y.; Dai, Y.; Fu, F. High-performance magnetic carbon materials in dye removal from aqueous solutions. *J. Solid State Chem.* **2016**, *239*, 265–273. [[CrossRef](#)]
78. Qian, F.; Zhu, X.; Liu, Y.; Hao, S.; Ren, Z.J.; Gao, B.; Zong, R.; Zhang, S.; Chen, J. Synthesis, characterization and adsorption capacity of magnetic carbon composites activated by CO₂: Implication for the catalytic mechanisms of iron salts. *J. Mater. Chem. A* **2016**, *4*, 18942–18951. [[CrossRef](#)]
79. Sun, Y.; Yue, Q.; Mao, Y.; Gao, B.; Gao, Y.; Huang, L. Enhanced adsorption of chromium onto activated carbon by microwave-assisted H₃PO₄ mixed with Fe/Al/Mn activation. *J. Hazard. Mater.* **2014**, *265*, 191–200. [[CrossRef](#)] [[PubMed](#)]
80. Arroyo-Gómez, J.J.; Villarroel-Rocha, D.; de Freitas-Araújo, K.C.; Martínez-Huitle, C.A.; Sapag, K. Applicability of activated carbon obtained from peach stone as an electrochemical sensor for detecting caffeine. *J. Electroanal. Chem.* **2018**, *822*, 171–176. [[CrossRef](#)]
81. Wang, L.; Sun, F.; Gao, J.; Pi, X.; Pei, T.; Qie, Z.; Zhao, G.; Qin, Y. A novel melt infiltration method promoting porosity development of low-rank coal derived activated carbon as supercapacitor electrode materials. *J. Taiwan Inst. Chem. Eng.* **2018**, *91*, 588–596. [[CrossRef](#)]
82. Yu, I.K.M.; Xiong, X.; Tsang, D.C.W.; Wang, L.; Hunt, A.J.; Song, H.; Shang, J.; Ok, Y.S.; Poon, C.S. Aluminium-biochar composites as sustainable heterogeneous catalysts for glucose isomerisation in a biorefinery. *Green Chem.* **2019**, *21*, 1267–1281. [[CrossRef](#)]
83. Yang, X.; Yu, I.K.M.; Cho, D.W.; Chen, S.S.; Tsang, D.C.W.; Shang, J.; Yip, A.C.K.; Wang, L.; Ok, Y.S. Tin-Functionalized Wood Biochar as a Sustainable Solid Catalyst for Glucose Isomerization in Biorefinery. *ACS Sustain. Chem. Eng.* **2019**, *7*, 4851–4860. [[CrossRef](#)]
84. Wan, Z.; Sun, Y.; Tsang, D.C.W.; Yu, I.K.M.; Fan, J.; Clark, J.H.; Zhou, Y.; Cao, X.; Gao, B.; Ok, Y.S. A sustainable biochar catalyst synergized with copper heteroatoms and CO₂ for singlet oxygenation and electron transfer routes. *Green Chem.* **2019**, *21*, 4800–4814. [[CrossRef](#)]
85. Boudou, J.P.; Bégin, D.; Alain, E.; Furdin, G.; Maréché, J.F.; Albiniaik, A. Effects of FeCl₃ (intercalated or not in graphite) on the pyrolysis of coal or coal tar pitch. *Fuel* **1998**, *77*, 601–606. [[CrossRef](#)]

86. Mohanty, K.; Das, D.; Biswas, M.N. Preparation and characterization of activated carbons from *Sterculia alata* nutshell by chemical activation with zinc chloride to remove phenol from wastewater. *Adsorption* **2006**, *12*, 119–132. [[CrossRef](#)]
87. Fu, K.; Yue, Q.; Gao, B.; Wang, Y.; Li, Q. Activated carbon from tomato stem by chemical activation with FeCl₂. *Colloids Surf. A Physicochem. Eng. Asp.* **2017**, *529*, 842–849. [[CrossRef](#)]
88. Chiu, K.L.; Ng, D.H.L. Synthesis and characterization of cotton-made activated carbon fiber and its adsorption of methylene blue in water treatment. *Biomass Bioenergy* **2012**, *46*, 102–110. [[CrossRef](#)]
89. Xu, Z.; Zhang, T.; Yuan, Z.; Zhang, D.; Sun, Z.; Huang, Y.X.; Chen, W.; Tian, D.; Deng, H.; Zhou, Y. Fabrication of cotton textile waste-based magnetic activated carbon using FeCl₃ activation by the Box-Behnken design: Optimization and characteristics. *RSC Adv.* **2018**, *8*, 38081–38090. [[CrossRef](#)]
90. Xu, Z.; Tian, D.; Sun, Z.; Zhang, D.; Zhou, Y.; Chen, W.; Deng, H. Highly porous activated carbon synthesized by pyrolysis of polyester fabric wastes with different iron salts: Pore development and adsorption behavior. *Colloids Surf. A Physicochem. Eng. Asp.* **2019**, *565*, 180–187. [[CrossRef](#)]
91. Liu, W.J.; Tian, K.; He, Y.R.; Jiang, H.; Yu, H.Q. High-yield harvest of nanofibers/mesoporous carbon composite by pyrolysis of waste biomass and its application for high durability electrochemical energy storage. *Environ. Sci. Technol.* **2014**, *48*, 13951–13959. [[CrossRef](#)]
92. Dastgheib, S.A.; Ren, J.; Rostam-Abadi, M.; Chang, R. Preparation of functionalized and metal-impregnated activated carbon by a single-step activation method. *Appl. Surf. Sci.* **2014**, *290*, 92–101. [[CrossRef](#)]
93. Luo, J.J.; Lu, J.; Niu, Q.; Chen, X.; Wang, Z.; Zhang, J. Preparation and characterization of benzoic acid-modified activated carbon for removal of gaseous mercury chloride. *Fuel* **2015**, *160*, 440–445. [[CrossRef](#)]
94. Prakash, R.; Mishra, A.K.; Roth, A.; Kübel, C.; Scherer, T.; Ghafari, M.; Hahn, H.; Fichtner, M. A ferrocene-based carbon-iron lithium fluoride nanocomposite as a stable electrode material in lithium batteries. *J. Mater. Chem.* **2010**, *20*, 1871–1876. [[CrossRef](#)]
95. Moulder, J.F.; Stickle, W.F.; Sobol, P.E.; Bomben, K.D. *Handbook of X-ray Photoelectron Spectroscopy*; Perkin-Elmer: Eden Prairie, MN, USA, 1992; ISBN 0962702625.
96. Volgmann, K.; Voigts, F.; Maus-Friedrichs, W. The interaction of oxygen molecules with iron films studied with MIES, UPS and XPS. *Surf. Sci.* **2010**, *604*, 906–913. [[CrossRef](#)]
97. Murad, E.; Johnston, J.H. *Mössbauer Spectroscopy Applied to Inorganic Chemistry*; Long, G.J., Grandjean, F., Eds.; Plenum Press: New York, NY, USA, 1984; pp. 507–582. ISBN 9780306430732.
98. Schaaf, P.; Wiesen, S.; Gonser, U. Mössbauer study of iron carbides: Cementite (Fe, M)₃C (M = Cr, Mn) with various manganese and chromium contents. *Acta Metall. Mater.* **1992**, *40*, 373–379. [[CrossRef](#)]
99. Rocha, L.S.; Pereira, D.; Sousa, É.; Otero, M.; Esteves, V.I.; Calisto, V. Recent advances on the development and application of magnetic activated carbon and char for the removal of pharmaceutical compounds from waters: A review. *Sci. Total Environ.* **2020**, *718*, 137272. [[CrossRef](#)] [[PubMed](#)]
100. Feng, Z.; Chen, H.; Li, H.; Yuan, R.; Wang, F.; Chen, Z.; Zhou, B. Preparation, characterization, and application of magnetic activated carbon for treatment of biologically treated papermaking wastewater. *Sci. Total Environ.* **2020**, *713*, 136423. [[CrossRef](#)] [[PubMed](#)]
101. Tang, Y.; Chen, Q.; Li, W.; Xie, X.; Zhang, W.; Zhang, X.; Chai, H.; Huang, Y. Engineering magnetic N-doped porous carbon with super-high ciprofloxacin adsorption capacity and wide pH adaptability. *J. Hazard. Mater.* **2020**, *388*, 122059. [[CrossRef](#)] [[PubMed](#)]
102. Zhou, Y.; Liu, X.; Tang, L.; Zhang, F.; Zeng, G.; Peng, X.; Luo, L.; Deng, Y.; Pang, Y.; Zhang, J. Insight into highly efficient co-removal of p-nitrophenol and lead by nitrogen-functionalized magnetic ordered mesoporous carbon: Performance and modelling. *J. Hazard. Mater.* **2017**, *333*, 80–87. [[CrossRef](#)] [[PubMed](#)]
103. Zhao, H.; Cheng, Y.; Lv, H.; Ji, G.; Du, Y. A novel hierarchically porous magnetic carbon derived from biomass for strong lightweight microwave absorption. *Carbon N. Y.* **2019**, *142*, 245–253. [[CrossRef](#)]
104. Zhang, M.; Gao, B.; Varnosfaderani, S.; Hebard, A.; Yao, Y.; Inyang, M. Preparation and characterization of a novel magnetic biochar for arsenic removal. *Bioresour. Technol.* **2013**, *130*, 457–462. [[CrossRef](#)]
105. Nethaji, S.; Sivasamy, A.; Mandal, A.B. Preparation and characterization of corn cob activated carbon coated with nano-sized magnetite particles for the removal of Cr(VI). *Bioresour. Technol.* **2013**, *134*, 94–100. [[CrossRef](#)]
106. Mohan, D.; Sarswat, A.; Singh, V.K.; Alexandre-Franco, M.; Pittman, C.U. Development of magnetic activated carbon from almond shells for trinitrophenol removal from water. *Chem. Eng. J.* **2011**, *172*, 1111–1125. [[CrossRef](#)]

107. Cui, H.J.; Cai, J.K.; Zhao, H.; Yuan, B.; Ai, C.; Fu, M.L. One step solvothermal synthesis of functional hybrid γ -Fe₂O₃/carbon hollow spheres with superior capacities for heavy metal removal. *J. Colloid Interface Sci.* **2014**, *425*, 131–135. [[CrossRef](#)]
108. Ahmed, M.J.; Dhedan, S.K. Equilibrium isotherms and kinetics modeling of methylene blue adsorption on agricultural wastes-based activated carbons. *Fluid Phase Equilib.* **2012**, *317*, 9–14. [[CrossRef](#)]
109. Rashid, J.; Tehreem, F.; Rehman, A.; Kumar, R. Synthesis using natural functionalization of activated carbon from pumpkin peels for decolourization of aqueous methylene blue. *Sci. Total Environ.* **2019**, *671*, 369–376. [[CrossRef](#)] [[PubMed](#)]
110. Liu, Q.-X.; Zhou, Y.-R.; Wang, M.; Zhang, Q.; Ji, T.; Chen, T.-Y.; Yu, D.-C. Adsorption of methylene blue from aqueous solution onto viscose-based activated carbon fiber felts: Kinetics and equilibrium studies. *Adsorpt. Sci. Technol.* **2019**, *37*, 312–332. [[CrossRef](#)]
111. Bedin, K.C.; Souza, I.P.A.F.; Cazetta, A.L.; Spessato, L.; Ronix, A.; Almeida, V.C. CO₂-spherical activated carbon as a new adsorbent for Methylene Blue removal: Kinetic, equilibrium and thermodynamic studies. *J. Mol. Liq.* **2018**, *269*, 132–139. [[CrossRef](#)]
112. Li, C.; Lu, J.; Li, S.; Tong, Y.; Ye, B. Synthesis of Magnetic Microspheres with Sodium Alginate and Activated Carbon for Removal of Methylene Blue. *Materials* **2017**, *10*, 84. [[CrossRef](#)] [[PubMed](#)]
113. Tang, D.; Zheng, Z.; Lin, K.; Luan, J.; Zhang, J. Adsorption of p-nitrophenol from aqueous solutions onto activated carbon fiber. *J. Hazard. Mater.* **2007**, *143*, 49–56. [[CrossRef](#)] [[PubMed](#)]
114. Ahmad, F.; Daud, W.M.A.W.; Ahmad, M.A.; Radzi, R. Using cocoa (*Theobroma cacao*) shell-based activated carbon to remove 4-nitrophenol from aqueous solution: Kinetics and equilibrium studies. *Chem. Eng. J.* **2011**, *178*, 461–467. [[CrossRef](#)]
115. Ahmaruzzaman, M.; Laxmi Gayatri, S. Batch adsorption of 4-nitrophenol by acid activated jute stick char: Equilibrium, kinetic and thermodynamic studies. *Chem. Eng. J.* **2010**, *158*, 173–180. [[CrossRef](#)]
116. Zheng, H.; Guo, W.; Li, S.; Chen, Y.; Wu, Q.; Feng, X.; Yin, R.; Ho, S.H.; Ren, N.; Chang, J.S. Adsorption of p-nitrophenols (PNP) on microalgal biochar: Analysis of high adsorption capacity and mechanism. *Bioresour. Technol.* **2017**, *244*, 1456–1464. [[CrossRef](#)]
117. Shi, Z.L.; Liu, F.M.; Yao, S.H. Adsorptive removal of phosphate from aqueous solutions using activated carbon loaded with Fe(III) oxide. *Xinxing Tan Cailiao N. Carbon Mater.* **2011**, *26*, 299–306. [[CrossRef](#)]
118. Dabrowski, A.; Podkościelny, P.; Hubicki, Z.; Barczak, M. Adsorption of phenolic compounds by activated carbon—A critical review. *Chemosphere* **2005**, *58*, 1049–1070. [[CrossRef](#)]
119. García-Mateos, F.J.; Ruiz-Rosas, R.; Marqués, M.D.; Cotoruelo, L.M.; Rodríguez-Mirasol, J.; Cordero, T. Removal of paracetamol on biomass-derived activated carbon: Modeling the fixed bed breakthrough curves using batch adsorption experiments. *Chem. Eng. J.* **2015**, *279*, 18–30. [[CrossRef](#)]
120. Mestre, A.S.; Pires, J.; Nogueira, J.M.F.; Carvalho, A.P. Activated carbons for the adsorption of ibuprofen. *Carbon N. Y.* **2007**, *45*, 1979–1988. [[CrossRef](#)]
121. Wang, X.S.; Chen, L.F.; Li, F.Y.; Chen, K.L.; Wan, W.Y.; Tang, Y.J. Removal of Cr(VI) with wheat-residue derived black carbon: Reaction mechanism and adsorption performance. *J. Hazard. Mater.* **2010**, *175*, 816–822. [[CrossRef](#)] [[PubMed](#)]
122. Fan, L.; Luo, C.; Sun, M.; Qiu, H. Synthesis of graphene oxide decorated with magnetic cyclodextrin for fast chromium removal. *J. Mater. Chem.* **2012**, *22*, 24577–24583. [[CrossRef](#)]
123. Zheng, Y.M.; Liu, T.; Jiang, J.; Yang, L.; Fan, Y.; Wee, A.T.S.; Chen, J.P. Characterization of hexavalent chromium interaction with *Sargassum* by X-ray absorption fine structure spectroscopy, X-ray photoelectron spectroscopy, and quantum chemistry calculation. *J. Colloid Interface Sci.* **2011**, *356*, 741–748. [[CrossRef](#)]
124. Li, L.; Fan, L.; Sun, M.; Qiu, H.; Li, X.; Duan, H.; Luo, C. Adsorbent for chromium removal based on graphene oxide functionalized with magnetic cyclodextrin-chitosan. *Colloids Surf. B Biointerfaces* **2013**, *107*, 76–83. [[CrossRef](#)]
125. Siddique, A.; Nayak, A.K.; Singh, J. Synthesis of FeCl₃-activated carbon derived from waste *Citrus limetta* peels for removal of fluoride: An eco-friendly approach for the treatment of groundwater and bio-waste collectively. *Groundw. Sustain. Dev.* **2020**, *10*, 100339. [[CrossRef](#)]
126. Peñas-Garzón, M.; Gómez-Avilés, A.; Bedia, J.; Rodríguez, J.J.; Belver, C. Effect of activating agent on the properties of TiO₂/activated carbon heterostructures for solar photocatalytic degradation of acetaminophen. *Materials* **2019**, *12*, 378. [[CrossRef](#)]

127. Peñas-Garzón, M.; Gómez-Avilés, A.; Belver, C.; Rodríguez, J.J.; Bedia, J. Degradation pathways of emerging contaminants using TiO₂-activated carbon heterostructures in aqueous solution under simulated solar light. *Chem. Eng. J.* **2020**, *124*, 867. [[CrossRef](#)]
128. Lin, Z.; Goikolea, E.; Balducci, A.; Naoi, K.; Taberna, P.L.; Salanne, M.; Yushin, G.; Simon, P. Materials for supercapacitors: When Li-ion battery power is not enough. *Mater. Today* **2018**, *21*, 419–436. [[CrossRef](#)]
129. Gu, W.; Yushin, G. Review of nanostructured carbon materials for electrochemical capacitor applications: Advantages and limitations of activated carbon, carbide-derived carbon, zeolite-templated carbon, carbon aerogels, carbon nanotubes, onion-like carbon, and graphene. *Wiley Interdiscip. Rev. Energy Environ.* **2014**, *3*, 424–473. [[CrossRef](#)]
130. Sevilla, M.; Mokaya, R. Energy storage. In *Energy and Environmental Science*; Royal Society of Chemistry: London, UK, 2014; Volume 7, pp. 1250–1280.
131. Yudasaka, M.; Kikuchi, R. Graphitization of Carbonaceous Materials by Ni, Co and Fe. In *Supercarbon—Synthesis, Properties and Applications*; Springer: Berlin, Germany, 1998; ISBN 978-3-642-08405-8.
132. Sajitha, E.P.; Prasad, V.; Subramanyam, S.V.; Eto, S.; Takai, K.; Enoki, T. Synthesis and characteristics of iron nanoparticles in a carbon matrix along with the catalytic graphitization of amorphous carbon. *Carbon N. Y.* **2004**, *42*, 2815–2820. [[CrossRef](#)]
133. Zhai, D.; Du, H.; Li, B.; Zhu, Y.; Kang, F. Porous graphitic carbons prepared by combining chemical activation with catalytic graphitization. *Carbon N. Y.* **2011**, *49*, 725–729. [[CrossRef](#)]
134. Thambiliyagodage, C.J.; Ulrich, S.; Araujo, P.T.; Bakker, M.G. Catalytic graphitization in nanocast carbon monoliths by iron, cobalt and nickel nanoparticles. *Carbon N. Y.* **2018**, *134*, 452–463. [[CrossRef](#)]
135. Liu, D.; Zhao, X.; Su, R.; Hao, Z.; Jia, B.; Li, S.; Dong, L. Highly porous graphitic activated carbons from lignite via microwave pretreatment and iron-catalyzed graphitization at low-temperature for supercapacitor electrode materials. *Processes* **2019**, *7*, 300. [[CrossRef](#)]



© 2020 by the authors. Licensee MDPI, Basel, Switzerland. This article is an open access article distributed under the terms and conditions of the Creative Commons Attribution (CC BY) license (<http://creativecommons.org/licenses/by/4.0/>).